Dynamics of photoinduced bulk and surface reactions involving semiconductors characterized by time resolved spectroscopy techniques (2015–2018)

Carsten Günnemann,[a] Mariano Curti,*[a] Jenny Schneider[b] and Detlef W. Bahnemann*[a,c]

DOI: 10.1039/9781788016520-00122

Time-resolved spectroscopic techniques represent a valuable set of tools for the analysis of photoinduced processes in semiconductors. We present here an overview of the underlying principles and of the insights that can be obtained from them, discuss different strategies for the analysis of transient decay kinetics, and highlight interesting examples from recent years as well as seminal works in the field.

1 Introduction

Materials of many semiconductor systems show the ability to directly convert light energy into chemical or electrical energy. Under band gap excitation of a semiconductor particle, the generation of the species responsible for photocatalysis occurs: electrons in the conduction band and positive holes in the valence band. Accordingly, the particle acts as a short-circuit electrode and is able to initiate oxidation and reduction processes of adsorbed substrates. The energy of the conduction and valence band, as well as other physical and structural properties of the semiconductor, control the reaction course of heterogeneous electron transfer at the surface. Understanding the sequence of events that occurs following the absorption of a photon and the correlation of the charge carrier dynamics to the material properties is a key to our understanding of photochemical reactions.

Time-resolved techniques allow to trace the ''fate'' and the pathways of the photogenerated species in semiconductors. The most interesting aspect of transient techniques, as implied by their name, is their time-resolved nature for very short scales. They are therefore a perfect match for photocatalytic processes, where the involved species are usually short-lived. Consequently, after their generation caused by the pulsed light excitation, a sharp decrease in their concentration will be observed. The concentration change as a function of time can be probed by monitoring different physical properties such as luminescence, absorption changes,

[a]*Institut für Technische Chemie, Gottfried Wilhelm Leibniz Universität Hannover, Callinstrasse 3, 30167 Hannover, Germany. E-mail: curti@iftc.uni-hannover.de; bahnemann@iftc.uni-hannover.de*
[b]*Department of Chemistry, University of North Carolina at Chapel Hill, 27599 Chapel Hill, USA*
[c]*Laboratory ''Photoactive Nanocomposite Materials'', Saint-Petersburg State University, Ulyanovskaya str. 1, Peterhof, 198504 Saint Petersburg, Russia*

conductivity, *etc.* In particular, the acquisition of differential absorbance (ΔA) spectra in the so-called transient absorption spectroscopy (TAS) has been used as a valuable technique to monitor the dynamics of free and trapped charge carriers photogenerated in different semiconductor nanomaterials. However, the interpretation and understanding of the physical properties observed by time-resolved optical spectroscopy remains an important and frequently far from trivial scientific task.

Several publications have been dedicated to this research area during the past 10 years and it is by no means the purpose of our present chapter to give a comprehensive overview of the field. The chapter starts with the basic principles of the time-resolved techniques and presents the technological progress of spectral and temporal resolutions providing specific study cases. The highlight of the chapter is the discussion of the mathematical and physical meaning of the transient decay kinetics and its importance for the mechanistic understanding of photocatalytic processes and for the design of efficient and tailored photocatalysts. Hopefully, this overview will be helpful to those working in the field and will, moreover, stimulate new research activities aiming to answer some of the central scientific questions that are still unresolved to date.

2 Principle and study cases of time-resolved spectroscopy

Transient absorption (TA) and emission spectroscopy techniques are well-established methods to study dynamic processes in a wide range of solar energy conversion materials. Time-resolved spectroscopy as we know it today was developed in the 1950s and early 1960s as flash photolysis and relaxation methods, a development that culminated with the Nobel Prize in Chemistry 1967 to Porter, Norrish, and Eigen.[1] The fundamental idea of the method is to use a pulsed excitation source, $h\nu_e$, to disturb the ground state of the system and to follow the course of the photo-reaction by monitoring the optical changes of the system by the analyzing light, $h\nu_a$, fired at a known delay after the first (Fig. 1). The analyzing light intensity before I_0 and after the excitation I_t of the sample is detected and passed to the transient recorder, oscilloscope, which allows the temporal resolution of the signal. Subsequently, the transient signal, ΔA, is recorded as a function of delay time following the rise and decay kinetics of the reaction intermediate which absorbs the probe light. In transient emission spectroscopy the change of the emitted light intensity with and without the excitation is detected in the absence of the analyzing light.

With time-resolved techniques available today, virtually any molecule and/or material can be excited to initiate the process, and most molecular and material absorptive or emissive responses monitored down to femtosecond time scales and beyond. Reviews and books provide excellent descriptions of most time-resolved techniques.[2–5] In the next subsections we will focus on the different detection regimes of the fast processes photo-initiated in the semiconductor materials, providing study cases from the literature.

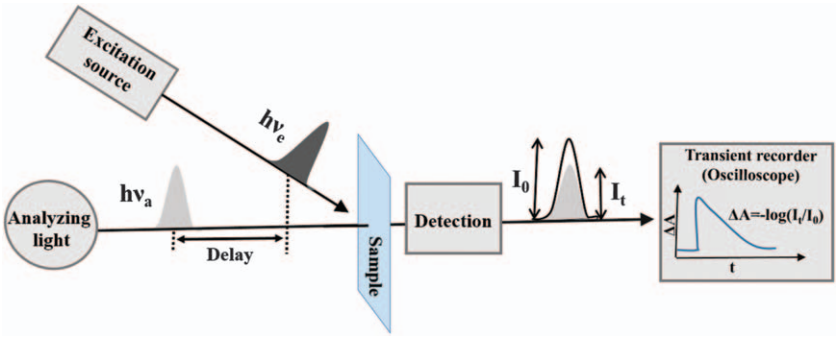

Fig. 1 Principle of TA spectroscopy. Optical excitation $h\nu_e$ of a sample leads to the change in the analyzing light $h\nu_a$ intensity from I_0 to I_t, which is monitored in temporal resolution by the transient recorder, oscilloscope. The transient signal, ΔA, represents the rise and decay of the formed intermediate.

2.1 Detection mode: absorption, emission, transmission, reflection

The electrons and holes photogenerated in a semiconductor alter its optical properties. The generated charge carriers undergo reactions with certain lattice or terminal atoms upon formation of the intermediate species, which exhibit specific optical properties. For example, in TiO_2 the photogenerated electrons tend to be trapped at Ti^{4+} centers. This results in the formation of an intermediate, Ti^{3+}, the lifetime of which is determined by the recombination with the holes and by the interfacial transfer to the molecules adsorbed at the surface.[6] Transient absorption spectroscopy and time-resolved photoluminescence spectroscopy, TRPLS, allow tracking of the reaction dynamics of the generated species by measuring the change in the intensity of either transmitted or diffuse reflected light caused by absorption, for the former, and by measuring the change in the intensity of emitted light, for the latter.[5] Fig. 2 shows an example of the detection of an intermediate formed by the trapping of the electron. In the TAS experiment the absorption of the analyzing light by the intermediate formed upon excitation induces the electronic transition, which did not exist in the ground state. Hence, the observed ΔA, a difference between the ground state absorption and photoinduced absorption, represents the absorbance of the intermediate. If the experiments were conducted in the transmission mode, ΔA is direct proportional to the concentration c of the photogenerated species in accordance with the Beer-Lambert law:

$$\Delta A = -\log(I_t/I_0) = \varepsilon c d \quad (1)$$

where ε is the extinction coefficient of the formed intermediate and d the optical path length.

To obtain quantitative information from TAS experiments it is necessary to measure the extinction coefficients of the species formed in the semiconductor upon excitation. For example, Durrant *et al.*[7] applied a spectroelectrochemical method to determine the extinction coefficient of the electron and holes in TiO_2. In general, TAS provides useful information about various factors affecting the photocatalytic

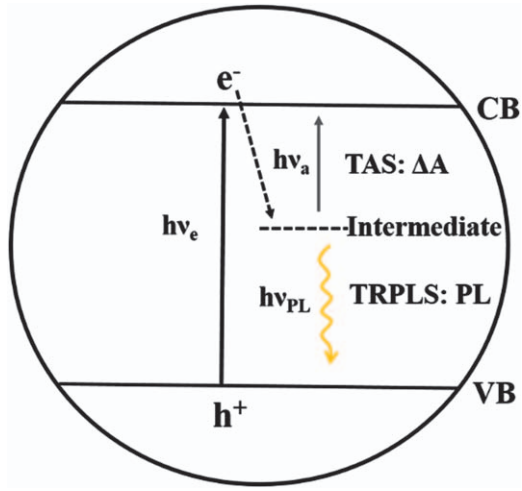

Fig. 2 Optical excitation, $h\nu_e$, of a semiconductor leads to the formation of an electron in the conduction band, CB, and a hole in the valence band, VB. The trapping of the electron results in the formation of an intermediate, which can be detected either by means of TAS *via* measuring the change of the analyzing light, $h\nu_a$, absorption or by means of TRPLS *via* monitoring the emitted light, $h\nu_{pl}$.

performance of semiconductors, such as defects, electronic structures, and the separation and recombination of photoinduced charge carriers. Recently, Kafizas *et al.*[8] observed by means of TAS that the $WO_3/BiVO_4$ junction improves hole accumulation at the surface with respect to $BiVO_4$ alone. The lifetime of the holes was over time scales relevant to photocatalytic water oxidation. Previously, it has been shown that the lifetime of the holes can be also extended upon applied positive bias. Under these conditions the holes photogenerated in TiO_2 and Fe_2O_3 showed ~100% selectivity toward the evolution of O_2.[9]

The time-resolved photoluminescence spectroscopy is widely applied to determine the energetic distribution of midband gap states among the tracking of the radiative recombination of photogenerated charge carriers.[5] The energetic positions of the trapped charge carriers determine their ability to induce redox reactions and, hence, the photocatalytic performance of the semiconductor. Fig. 2 demonstrates the detection of the radiative recombination of the trapped electron with the valence band hole by means of TRPLS. For both, anatase and rutile TiO_2 the photoluminescence (PL) spectra in the visible and the near-IR- wavelength range, respectively, have been reported, whereas the PL for anatase was related to self-trapped excitons, and, for rutile, to intrinsic sites or to surface bound species.[10–12] The surface trapped electrons in anatase are found to be located about 0.7–1.6 eV below the conduction band edge, while the trapped holes are about 1.8–2.5 eV below the conduction band edge. Yamada *et al.*[13] investigated the charge carrier recombination dynamics in rutile and anatase TiO_2 single crystals employing a combination of time-resolved PL and TA measurements and found longer lifetimes for electrons in anatase (>few ms) in comparison to rutile (24 ns), while the decay for the holes in both crystal phases occurs on the

nanosecond time scale. The shorter lifetime of the holes in anatase in comparison to the electrons indicate the former undergo additional recombination pathways, such as generation of peroxo-species by the dimerization reactions of the hydroxyl radicals. However, the authors claimed that the long-lived electrons in anatase are responsible for the better photocatalytic activity in comparison to rutile.

Most of the time-resolved studies on the reaction dynamics of the photogenerated charge carriers have been performed in transmission mode on transparent colloidal dispersions or on transparent films.[14–21] The data obtained from these studies were often used to explain the photocatalytic activities of opaque reaction media. Moreover, many reports have been published explaining different photocatalytic activities in terms of different recombination kinetics, although the latter ones were not measured. This established fact became a central point of a critical review recently written by Ohtani,[22] where he states: "*Thus, recombination has been used as an "almighty" card, but at the same time "ghost", for interpretation of photocatalytic activities without leading to progress in an understanding of photocatalysis and/or photocatalysts, since discussion with the term recombination is just an alternative description of experimental results.*".

Time-resolved diffuse reflectance spectroscopy, TRDRS, allows the observation of the charge carrier dynamics of photocatalyst powders or opaque suspensions. A major advantage is that the obtained kinetic data can be directly correlated with the outcome of the photocatalytic tests, since in both systems powdered samples are applied. The first successful report of TAS in diffuse reflectance mode on opaque samples was published by Kessler and Wilkinson in 1981.[23] The transient species were detected after excitation by monitoring the changes in the level of diffusely reflected light. The main difference to the technique used in transmission experiments is the geometrical arrangement of the analyzing light. Herein, the detector and the analyzing light are assembled to ensure that no specularly reflected light enters the detector and that the maximum amount of the diffusely reflected light is collected and analyzed as shown in Fig. 3. Since the diffusely reflected light has penetrated a substantial portion of the sample, it contains the information concerning

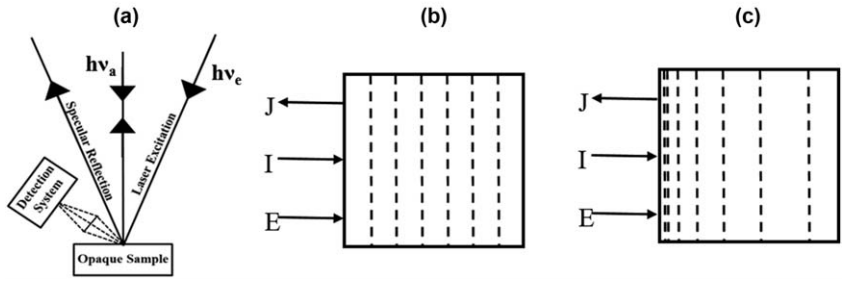

Fig. 3 (a) Schematic illustration of the sample geometry used in TRDRS. Homogeneous (b) and exponentially (c) falling-off concentration profile of the photogenerated transient species in TRDRS measurements (*E*: exciting light; *I*: incident monitoring light; *J*: reflected monitoring light).

its absorption. Further requirements for the arrangement of the components are described in detail elsewhere.[24–26]

For an optically dense sample studied by TRDRS the reflected light is measured. The reflectance, R, is defined as the quotient of the incident intensity of the analyzing light, I_0, at a wavelength λ_x and the diffuse reflected light, J_0: $R_0 = J_0/I_0$. If the laser excitation generates a transient species that has an absorption at a wavelength, λ_x, this will result in the decrease of J_0 to J_x, while I_0 remains constant. Hence, the reflectance will be reduced to R_x. In the case that the transient species has no reaction partner in the system a build-up of the transient occurs; otherwise, if any reaction proceeds, *e.g.*, recombination, reduction, oxidation, *etc.*, the disappearance of the species will lead to an increase of J_x and the decay of the transient can be followed until the original level of J_0 is approached. Mathematically, this can be summarized as:[25]

$$\Delta R = \frac{R_0 - R_x}{R_0} = 1 - R_T^x \text{ or } \Delta J = \frac{\frac{J_0}{I_0} - \frac{J_x}{I_0}}{\frac{J_0}{I_0}} = \frac{J_0 - J_x}{J_0} = 1 - J_T^x \qquad (2)$$

where R_T^x is defined as R_x/R_0 and J_T^x as J_x/J_0.

To assign the observed change in reflection after the pulse excitation to the TA and thus to a concentration of the formed intermediates two limiting types of transient concentration profiles should be considered, namely, the homogeneous and the exponentially falling-off profiles as depicted in Fig. 3.

Homogeneous distribution of the transient species (Fig. 3(a)) occurs at larger laser fluxes in diluted samples with a high ground state extinction coefficient at the exciting wavelength to ensure a high conversion percentage of the ground to the excited state. In this case the transient can be described using the Kubelka–Munk approach which relates the observed reflectance R to the absorption coefficient K and the scattering coefficient S:

$$\frac{(1-R)^2}{2R} = \frac{K}{S} \qquad (3)$$

as follows:

$$\Delta R_K = \frac{(1-R_x)^2}{2R_x} - \frac{(1-R_0)^2}{2R_0} = \frac{K_T}{S} \qquad (4)$$

where R_0 and R_x represent the reflection before and after laser excitation and K_T the TA. In a diffuse reflectance measurement, the value of R can be determined if the incident analyzing light intensity I_0 is known. The later one can be calculated from the experimentally measured value of J using a powder with a known value of R.

According to the Kubelka–Munk approach the absorption coefficient K exhibits a linear dependency on the concentration:[27]

$$K = \varepsilon c \qquad (5)$$

For relating the observed transient reflectance to the transient concentration c_T at any time after the flash the extinction coefficient of the ground state absorber ε_G and of the transient species ε_T should be considered:

$$\Delta R_K = \frac{K_T}{S} = \frac{2(\varepsilon_T - \varepsilon_G)c_T}{S} \tag{6}$$

However, it can be assumed that in the TRDRS the exponential distribution of the excited states prevails (Fig. 3(b)).[25] This is due to the fact that the experiments are mostly performed at such conditions at which the ratio of the number of absorber units to the number of the exciting photons is high, thus a low conversion percentage of the ground state to the transient state is expected. Here, eqn (6) cannot be applied. For the description of the exponentially falling-off concentration the system can be divided into a series of ''thin slices'' for which the Kubelka–Munk function is valid. Numerical solutions for this approach predict that a linear relationship exists between the reflectance change $(1 - R_T^x)$ and the total transient concentration at values of $(-R_T^x)$ below 0.1.[28]

There are several studies published on the charge carriers' dynamics monitored in TiO_2 powders. For example, Yamakata *et al.*[29] applied TRDRS in the visible to mid-IR range to explain the different photocatalytic activity of anatase and rutile TiO_2 powders. They found that in anatase TiO_2, a considerable number of free electrons survives longer than 1 ms, but they are deeply trapped within a few picoseconds in the case of rutile TiO_2 (Fig. 4). The authors concluded that the longer lifetime of free electrons is responsible for the higher activity for reduction processes on anatase TiO_2. The deep electron trapping in rutile TiO_2 elongates the lifetime of holes and promotes multihole processes such

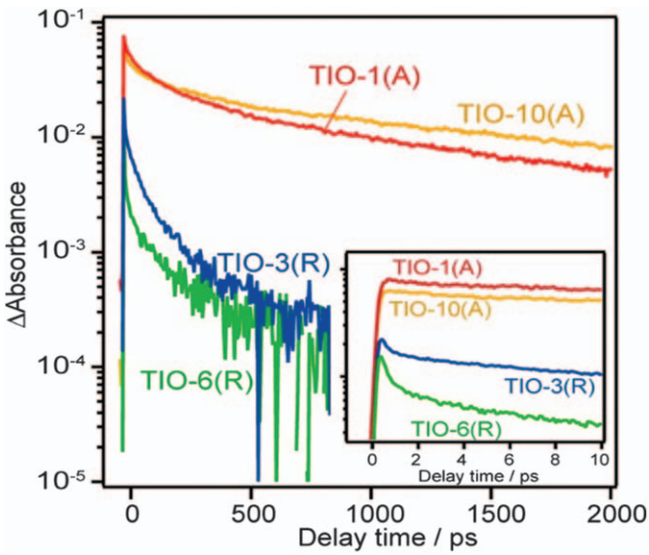

Fig. 4 Decay curves of free electrons in polycrystalline anatase and rutile TiO_2 samples measured in vacuum at 2000 cm^{-1}. Reproduced from ref. 29 with permission from American Chemical Society, Copyright 2015.

as water oxidation. However, the low reactivity of deeply trapped electrons fails to increase the overall activity.

Besides TiO_2, further powdered photocatalysts such as tantalates have been studied to elucidate the charge carrier dynamics.[30] For example, the kinetic data obtained by means of TRDRS explained the different photocatalytic behavior of phase pure $Ba_5Ta_4O_{15}$ and of a $Ba_5Ta_4O_{15}$–$Ba_3Ta_5O_{15}$ composite.[31] In the presence of methanol, for the pure phase $Ba_5Ta_4O_{15}$ the recombination of the charge carriers could not be prevented and the trapped electrons also recombine with the $^{\bullet}CH_2OH$ radical formed *via* the methanol oxidation by the trapped holes. However, in the composite, the electron can be stored in the system, the $^{\bullet}CH_2OH$ radical injects an electron into the conduction band of the second component of the composite, *i.e.*, $Ba_3Ta_5O_{15}$. Hence, the electrons are available for an extended period to induce reduction reactions.

However, by the experiments with the powders the laser excitation can induce irreversible changes of the sample more likely, in comparison to the experiments in suspension, where the solvent absorbs partially the photons coming out of the excitation source. Schneider *et al.*[32,33] observed irreversible changes of TiO_2 powders induced *via* the laser excitation in TRDRS, which has been related to the formation of nonreactive trapped electrons accompanied by the release of oxygen atoms from the TiO_2 matrix. The irreversible changes were identified by means of UV–Vis and electron paramagnetic resonance spectroscopies. Moreover, in the case of the pure anatase sample a phase transition of some TiO_2 nanoparticles located in the inner region from anatase to rutile occurred. Furthermore, it has been shown that the laser-induced irreversible changes of the sample can affect drastically the transient signals. In case of TiO_2 a considerable deceleration of the decay kinetics and a strong increase of the TA signal recorded in the wavelength region where the trapped holes absorb have been found. However, for anatase samples, such changes disappear at weak excitation conditions, while in the case of rutile they cannot be avoided.

2.2 Detection time: processes in femtosecond to microsecond time regime

The time resolution of the time-resolved spectroscopy is determined by the duration of the laser pulse, which should be faster than the photo-initiated processes, *e.g.* electron–hole recombination in a semiconductor. With the fast development of lasers, the time scales of the measurement extend nowadays from the microsecond to the femtosecond domain. The mode-locking lasers generate pulses, which allow the femto-to-subnanosecond resolution (ultrafast TAS), while Q-switched lasers are applied for experiments in the nano-to-millisecond time regime. The excitation pulse repetition rate is another important parameter and it must be low enough that the system relaxes to the starting ground state before the next pulse arrives. In nano-to-millisecond TAS the laser fires at a 1 Hz repetition frequency, while in ultrafast TAS the laser operates at typically 1 kHz. In experiments at such high repetition rate the annihilation of intermediates can occur. However, this can be prevented using the raster scanning across the sample between excitation pulses.

Furthermore, the time resolution of the measurements depends on the delay time between the excitation and probing pulses (see Fig. 1). In case of ultrafast TAS the maximum time delay is of a few nanoseconds, thus processes at longer time scales cannot be captured. However, this issue can be overcome by employing a dual-laser setup consisting of electronically synchronized Ti:sapphire amplifiers seeded by the same Ti:sapphire oscillator. Such a setup enables to measure the femtosecond to millisecond regime in a single experiment, as it has been shown by Kennis *et al.*[34] The authors applied this setup to study the charge carrier dynamics in bismuth vanadate ($BiVO_4$) on the femtosecond to microsecond time scales. As it is shown in Fig. 5, the trapping (rise of the transient signal) and the recombination (decay) of the charge carriers were monitored at 475 and 700 nm with the same experimental settings.

The time resolution of the nowadays available TAS allows to identify the time regime of the main photoinduced processes in various semiconductors. The time scales of charge carrier generation, trapping, recombination, and interfacial transfer are summarized in Fig. 6. Within the first few femtoseconds after the excitation, the formation of the charge carriers occurs, with the hole located in the valence band, VB, and the electron in the conduction band, CB. The generated charge carriers tend to be trapped very fast either in the bulk or at the surface. The trapping in the shallow traps is found to occur within 100 femtoseconds up to few picoseconds. The relaxation into the deeper traps occurs at longer time scales, *e.g.* for TiO_2 500 ps has been measured.[35] The lifetime of the photogenerated charge carriers varies. For example, the recombination between trapped and free charge carriers is very fast, in the picosecond to nanosecond time domain, while the recombination between the trapped charge carriers is slower extending into the microsecond range. Those charge carriers that survived the recombination, can undergo reactions with the adsorbed molecules at the surface. The time regime of the interfacial reactions varies depending on the type of the adsorbate, binding mode and whether the trapped or free charge carriers participate in the reaction. For example, the electron transfer from the CB

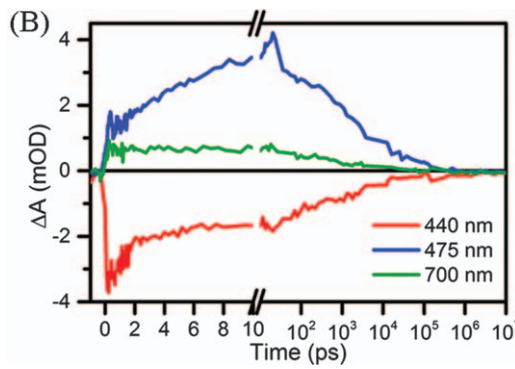

Fig. 5 TA traces at 440, 475, and 700 nm for $BiVO_4$ in air (excitation at 400 nm, 50 nJ, 1 kHz). The time axis is linear up to 10 ps and logarithmic from 10 ps to 10 μs. Reproduced from ref. 34 with permission from American Chemical Society, Copyright 2014.

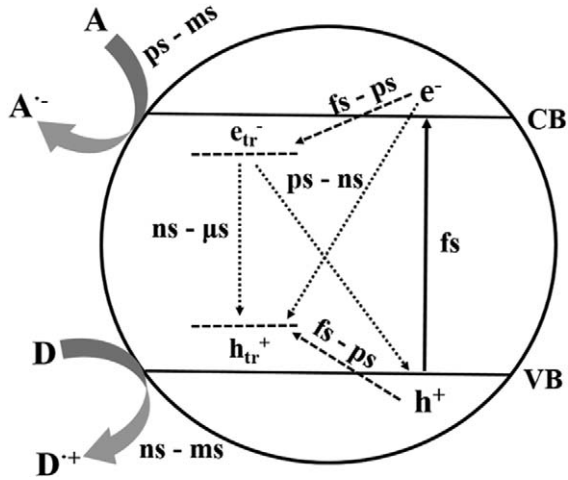

Fig. 6 Photoinduced processes in a semiconductor particle with their respective time-scales: charge carrier excitation (solid line), recombination (dotted line), trapping (dashed line) and interfacial charge transfer (block arrows). e^- and h^+ represent the free electrons and holes, respectively. e_{tr}^- and h_{tr}^+ represent the trapped electrons and holes, respectively. CB and VB correspond to the conduction and valence bands, respectively.

to noble metal nanoparticles is found to occur within a few picoseconds, while the reduction of oxygen is in the microsecond range.[36,37] The reaction of the holes with adsorbed water is the rate limiting process in the photocatalytic water splitting with the reaction time up to few milliseconds, while the oxidation of organic molecules is very fast, within a nanosecond.[38,39]

2.3 Detection range: UV–Vis, NIR, IR, microwave conductivity

The detection range is determined by the analyzing source and by the detector. For the nano-to-millisecond experiments, the analyzing light is typically provided by pulsed Xe arc lamps. If the lifetime of the process of interest is in the millisecond scale or above, probing can be afforded by a continuous light source. For ultrafast experiments the analyzing beam is generally produced by using a fraction of the laser pulse, which is used to produce a white light continuum. This is then delayed from the pump beam by a motorized translational stage. UV–Vis and near-IR probing light can be detected by a light detector such as the R928 photomultiplier with sensitivity from 185 to 900 nm. The light detectors such as silicon and InGaAs pin-photodiodes are sensitive in the 400–1000 nm region and 600–1600 nm region, respectively. Optical parametric amplification and white-light continuum generation techniques can also easily generate tunable or broad-band probe light. By introducing an IR generation option for the optical parametric amplifier (OPA), IR detectors such as mercury–cadmium–telluride (MCT, Hamamatsu, P3257-10) and some optical components, one can extend the visible-to-near-IR TA to a mid-IR wavelength range. More technical details are given in ref. 40.

Most of the intermediates photo-generated in the semiconductor and participating in photocatalytic reactions, *e.g.* hydroxyl radicals, absorb in

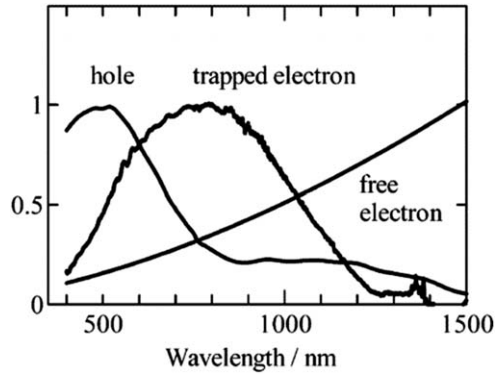

Fig. 7 The TA spectra of trapped holes, free electrons, and trapped electrons. Reproduced from ref. 20 with permission from American Chemical Society, Copyright 2004.

the UV–Vis wavelength range. The free charge carriers delocalized within the CB or VB show absorption in the IR near-IR region. Yoshihara *et al.*[20] were able to identify reactive species (trapped holes, trapped and free electrons) in nanocrystalline TiO_2 films in the wavelength range from 400 to 1500 nm (Fig. 7). We cover the assignment of signals to specific species in Section 3.

Time-resolved microwave conductivity (TRMC) provides another feasible technique to study the reaction dynamics of photogenerated charge carriers in semiconductors. TRMC is based on the measurement of the relative change of the microwave power reflected from the sample before and after the excitation. The photogenerated charge carriers formed upon excitation will induce changes in the sample's conductivity, thus resulting in changes of the microwave power reflected by the sample. For TiO_2, the interpretation of the observed TRMC signals is usually based on the assumption that the electrons have a much higher mobility than the holes; thus, the observed conductivity can be attributed to the presence of excess electrons in the conduction band. A recently published review by Colbeau-Justin *et al.* provides an overview concerning the use of time-resolved conductivity measurements for the detection of mobile electrons in different systems.[41]

Today, with the availability of large-scale facilities specializing in the generation of ultrashort pulses in a wide spectral range, like free electron lasers, or high power laser facilities, femtosecond pulses can be generated from THz frequencies to hard X-rays.[2] This enables the probing of light–matter interactions over a broad range of time-, energy-, and length-scales. For example, Baker *et al.*[42] applied femtosecond extreme ultraviolet (XUV) spectroscopy in conjunction with X-ray photoelectron spectroscopy (XPS) to study ultrafast surface electron dynamics with chemical state in NiO. XUV spectroscopy probes core-to-valence transitions, which are element specific and provide detailed electronic structure information, including the transient oxidation state of the Ni metal center. Using femtosecond pulses of XUV light produced by tabletop high harmonic generation enables direct observation of ultrafast electron dynamics in an optical pump, XUV probe experiment. The findings from

this study resolved important questions related to the mechanisms of carrier trapping and subsequent recombination in NiO and provided parameters for the design of efficient materials.

3 Signal assignment

As aforementioned, time-resolved techniques allow the spectroscopical characterization of photogenerated intermediates in semiconductors. The reaction dynamics of the intermediates participating in the photocatalytic reaction provide information on the reaction mechanism. However, before a kinetic analysis can be applied, the wavelength range where the photogenerated intermediates absorb needs to be identified. This can be derived from the TA spectra, which can be obtained from the TA signal monitored at different wavelengths. As an example, in Fig. 8 a TA decay, ΔA as the function of time recorded at three different wavelengths, λ, is shown. Directly after the excitation (0 μs) with the laser the highest value for ΔA is reached, evincing the formation of an intermediate that disappears due its reactivity, and ΔA decays to zero. The plot of ΔA at constant t for different wavelengths provides a two dimensional data array, ΔA ($t =$ constant, λ), called TA spectrum.

It is a real challenge to assign the optical transitions derived from the TA spectra to individual electronically excited states with corresponding chemical identity. The precise assignment of a TA is hindered by many factors such as the broadness and the overlap of the TA spectra, the distribution of the holes and electrons, the various trapping states, and the sensitivity of the TA spectra to the experimental conditions as well as to the chemical and physical properties of the investigated particles.

In the following we discuss the possible transitions of trapped holes, trapped electrons and free electrons. In general, free electrons are charge carriers that are delocalized within the CB. After the absorption of light the free electrons can be excited from a lower state in the CB to a higher state in the CB, known as an interband transition (Fig. 9,(1)). These transitions are usually observed in the IR wavelength range. The energy levels of the trapped charge carriers are normally located within the band gap. For the trapped electron the optical transition corresponds to the excitation from the trap state to the CB (Fig. 9,(2)). For TiO_2, the localized Ti^{3+} electrons undergo d–d transitions upon excitation.[43] The possible transitions of trapped holes are still a part of an ongoing controversy. The trapped hole represents a defect electron (missing electron at a certain energy state), however, in case of metal oxide photocatalysts the hole corresponds to an oxygen centered radical, which could originate either from terminal hydroxyl groups or lattice oxygen.[44] The TA of this radical can be attributed either to the transition from the trap state to the CB forming unstable O atoms in the lattice, or from the valence band to the trap state. Henderson *et al.* assumed that the latter transition may not be optically allowed.[45] However, recently published DFT calculations on TiO_2 demonstrated that the TA of the trapped holes is due to the transition of electrons from the valence band to the trap state (Fig. 9,(3)).[43]

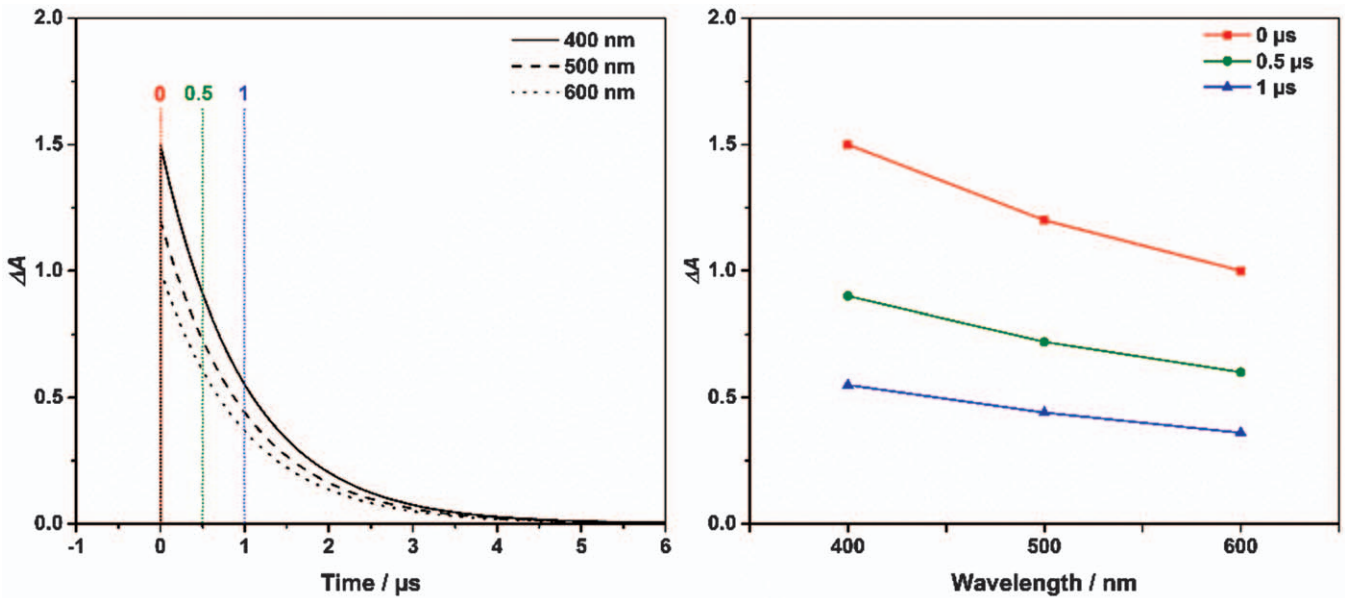

Fig. 8 (left) Plot of the TA decay, shown as ΔA against time, for the three example wavelengths 400 nm, 500 nm, and 600 nm. For obtaining spectra out of the decays the ΔA values at different time points are taken. The red (0 μs), green (0.5 μs), and blue (1 μs) lines represent three example time points. (right) The spectra for the three time points are constructed by plotting ΔA against the wavelength for the chosen time point.

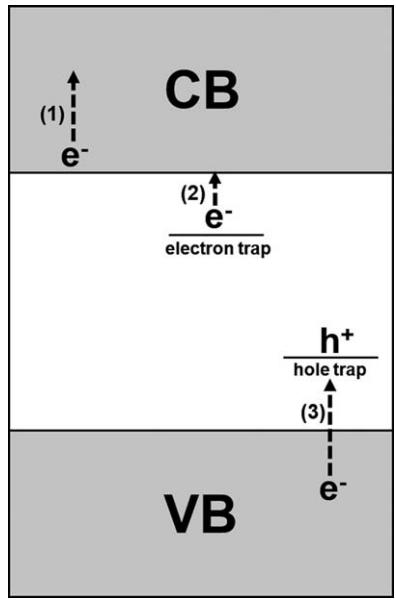

Fig. 9 Representation of the possible transitions of the free and trapped charge carriers, which occur after the absorption of light. Free electrons are excited to higher states in the CB (1), while trapped electrons are excited from the trap state to the CB (2). The absorption of a trapped hole is shown as an excitation of an electron in the VB to the hole trap state (3).

Table 1 Examples for typical chemical and electrochemical hole scavengers and electron scavengers taken from the literature.

	Hole scavengers	Electron scavengers
Chemical	Methanol[31]	Oxygen[37]
	Ethanol[37]	Methylviologen[15]
	Propanol[39]	Pt[15]
	Polyvinyl alcohol[15]	Ag^{+} [53]
	Na_2SO_3 [53]	Cu^{2+} [49]
Electrochemical	Cathodic bias[54]	Anodic bias[7]

Under inert atmosphere, both electrons and holes are present after the excitation of the sample, and as a result, the recorded TA spectra are broad and featureless. The addition of electron donors and acceptors allows the identification of the individual wavelength regions where photogenerated electrons and holes absorb. A typical scavenger for holes is methanol and a typical electron scavenger is oxygen. Further examples for electron and hole scavengers are given in Table 1. Methanol reacts with holes forming an α-hydroxyl radical in the first step (eqn (7)), while electrons and oxygen form a superoxide radical (eqn (8)).[37,46] For both reactions it can be seen that either the photogenerated electrons or the holes are consumed by the scavenger, thus preventing (or hindering) the recombination reaction.

$$CH_3OH + h^+ \rightarrow {}^{\bullet}CH_2OH + H^+ \quad (7)$$

$$O_2 + e^- \rightarrow O_2^{\bullet -} \quad (8)$$

In general, the use of hole and electron scavengers influences the chemical environment compared to an inert atmosphere. After the oxidation to the α-hydroxyl radical (eqn (7)), methanol can be further oxidized to formaldehyde (CH_2O). The oxidation to formaldehyde usually occurs by the injection of an electron into the CB, which is called current-doubling.[46] This process and the hole scavenging itself lead to the accumulation of electrons at the particle and to a downward band bending.[6] Thus the addition of methanol does not only scavenge the holes, since even the band bending itself is strongly affected by the alcohol. The current doubling effect is not only observed for methanol, but also for ethanol and propanol, which are commonly used as hole scavengers as well.[6] Oxygen, which is often used as electron scavenger, reacts slowly with the photogenerated electrons.[47] But to be an efficient electron scavenger the reaction of the photogenerated electrons with the electron acceptor should be faster than the recombination. Platinum is an alternative electron scavenger, which captures photogenerated electrons within a few picoseconds. However, an homogeneous deposition of Pt on the semiconductor surface is a challenge and it results mostly in an unequal distribution and the formation of islands.[48] The unequal distribution of Pt and its optical absorption are disadvantages for the application as an electron acceptor.[48] Further, silver cations, Ag^+, were applied as electron scavengers. Upon reaction with the photogenerated electrons Ag^+ is reduced to Ag.[49] However, the silver nanoparticles exhibit a strong plasmon absorption at around 430 nm, which is in the wavelength region where photogenerated holes absorb.[48,50] Cu^{2+} ions have as well the ability to scavenge the electrons, forming Cu^+ ions, which have the advantage that no light is absorbed at wavelengths longer than 350 nm.[49]

Furthermore, the photogenerated charge carriers can be scavenged electrochemically (Table 1). Under applied cathodic bias the holes are scavenged and under anodic bias the electrons are removed from the system. However, applying a bias to an electrode causes a band bending as well, as long as it is not equal to the flatband potential of the semiconductor.[51]

In summary, it is obvious that there is no optimal scavenger and every commonly used scavenger has its disadvantages. But still to determine where electrons and holes absorb a scavenger is indispensable, while it has always to be taken into account that the system is changed after the addition of the scavenger.[52]

An example for the detection of the photogenerated charge carriers in TiO_2 in the presence of electron and hole scavengers is shown in Fig. 10. After the addition of Pt, the TA of the trapped holes is observed with a maximum at 450 nm, while in the presence of polyvinyl alcohol the absorption of the holes decreases and the absorption of the trapped electrons appears red shifted in comparison to the holes.

As mentioned in Section 2, Yoshihara *et al.*[20] were able to identify trapped holes, trapped and free electrons in TiO_2 by means of TA measurements on nanocrystalline TiO_2 slides (Fig. 7). The absorption maximum at 520 nm has been attributed to the trapped holes, while the absorption at 770 nm corresponds to the trapped electrons. Free

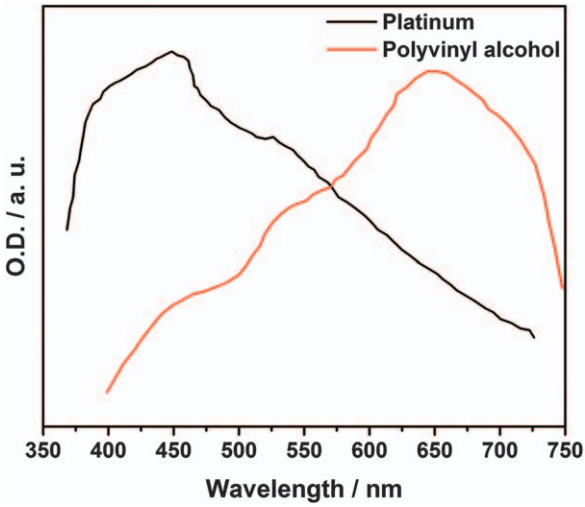

Fig. 10 TA spectra, shown as optical density against the wavelength, of a colloidal TiO_2 suspension with deposited platinum and after the addition of polyvinyl alcohol. Adapted from ref. 15 with permission from American Chemical Society, Copyright 1984.

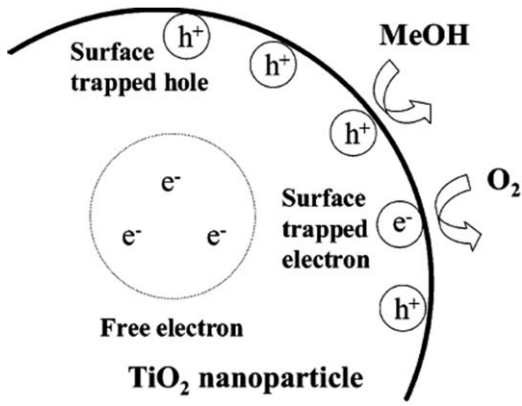

Fig. 11 Trapping of holes and electrons at the surface of a TiO_2 particle and free electrons moving in the bulk. Reproduced from ref. 20 with permission from American Chemical Society, Copyright 2004.

conduction band electrons exhibit an exponential increase in the absorbance proportional to λ^n, with $n = 1.7$. In addition, the authors concluded from their study that the free electrons are located in the bulk, while trapped charge carriers are localized at the surface (Fig. 11).

Furthermore, it is important to mention that the TA spectra of both electrons and holes are broad, and the behavior is indicative of the wide distribution of trapped states within the bandgap. This could be proven experimentally by Zhu *et al.*[55] The authors monitored the TA of the free electrons formed *via* the excitation with energies corresponding to certain transitions from the trapped state to the conduction band (Fig. 12).

TA measurements have been applied to study the formation of the photogenerated species in different semiconductors, in the presence of

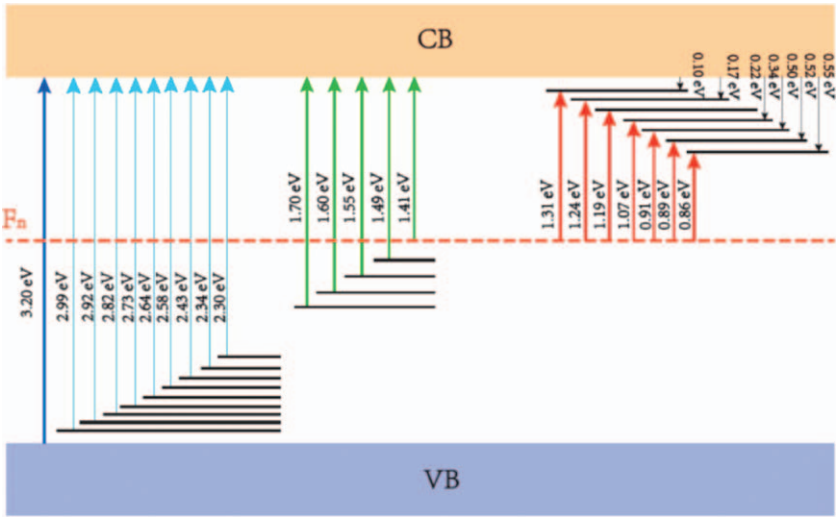

Fig. 12 Midgap energy states for trapped electrons in TiO_2. Reproduced from ref. 55 with permission from American Chemical Society, Copyright 2013.

various scavengers. Table 2 summarizes the TA wavelengths of the trapped charge carriers for different semiconductors.

4 Analysis of charge carrier decay kinetics

4.1 Overview

The time-resolved nature in very short scales of transient techniques make them a perfect match for photocatalytic processes, where the involved species are usually short-lived (Fig. 6). Consequently, after their generation caused by the laser pulse, a sharp decrease in their concentration will be observed. Both the functional shape of the decay and its lifetime provide valuable information on the underlying processes, and for that reason we delve in this section into different ways in which the decays can be analyzed.

The analysis of photocatalysts by TA spectroscopy starts with the assignment of the transient spectrum features to chemical species, such as photogenerated electron and holes, by using the procedures detailed in Section 3. As mentioned above, their high reactivity means their concentration will significantly decrease whatever the observation time window is, from femtoseconds to microseconds. As described in Section 2, the recombination of charge carriers usually proceeds much faster than electron transfer to or from appropriate scavengers. This means that, even in the presence of the latter, most photogenerated charge carriers will recombine, a fact evidenced by the low quantum yields shown by photocatalytic reactions (typically below a few percent[78]). Therefore, the decays in TA signals can be mainly attributed to electron–hole recombination. If the semiconductor's dielectric constant is high enough to shield charge carriers from each other, their intrinsic mobility will lead them through separate paths across the host particle. Ensuing

Table 2 TA maxima and ranges for trapped holes and electrons for different materials from the literature and the applied scavengers.

	Wavelength range		Scavengers		
Material	Trapped holes	Trapped electrons	Hole	Electrons	References
TiO_2 (Colloidal)	430–475 nm	650 nm	Polyvinyl alcohol Dichloroacetate Thiocyanate	Platinum	15, 56
TiO_2 (Film)	520 nm/1200 nm	770 nm	Methanol	—	20
TiO_2 (Powder)	470 nm	600 nm	—	—	57
$Ba_5Ta_4O_{15}$ (Powder)	310 nm	430 nm/650 nm	Methanol	—	31
CdS (Colloidal)	470–500 nm	300 nm/680 nm	Iodide Thiophenol	Zwitterionic viologen compound	58–61
$BiVO_4$ (Film)	550–700 nm	Not reported	Na_2SO_3 Water	$AgNO_3$ Fe^{3+}	53, 62
$BiVO_4$ (Powder)	580 nm	Not reported	Methanol	$AgNO_3$	63
α-Fe_2O_3 (Film)	600–650 nm	575 nm	Bias		64–66
WO_3 (Film)	430–500 nm	750–800 nm	Bias Methanol	$AgNO_3$ Bias	21, 67, 68
$BiFeO_3$ (Film)	Not reported	~539 nm (free)	—	—	69
$SrTiO_3$ (Powder/crystal)	500–689 nm	885–909 nm/4000 nm	Methanol	Oxygen	30, 70, 71
ZnO (Colloidal)	Not reported	700 nm	—	N_2O	72
CdSe	1300–1938 nm	900–1300 nm/2480 nm	1-Octanethiol	1,4-Benzoquinone	73, 74
g-C_3N_4 (Particles)	Not reported	500–1250 nm	Triethanolamine Methanol Oxalate	Platinum Sulfate Persulfate Nitrate Ag^+	75–77

encounters of oppositely charged carriers will lead to their recombination, which can then be thought of as a bimolecular process. It follows, from chemical intuition, that the kinetics of the process would be governed by a second-order rate law:

$$[c](t) = \frac{[c]_{t=0}}{[c]_{t=0} k_r t + 1} \tag{9}$$

where $[c](t)$ represents the charge carrier (electron or hole) concentration at time t, $[c]_{t=0}$ its concentration at $t = 0$ (*i.e.* right after the laser pulse), and k_r the second-order rate constant. Second-order kinetic profiles have indeed been observed in TA studies of different photocatalysts. The model, however, predicts that the charge carrier concentration approaches zero at long times, in contrast with typical observations. This long-lived absorption has thus been accounted for by including an additional term f,[79] constant during the measurement window. This results in a functional behavior termed "second-order with a baseline":

$$[c](t) = \frac{[c]_{t=0}}{[c]_{t=0} k_r t + 1} + f \tag{10}$$

This function is, possibly, the most widely applied in the analysis of TA decays. It has been observed, however, that changes in the experimental parameters such as the laser pulse intensity or the semiconductor's particle size (which ultimately define the average number of photogenerated charge carriers per particle) can strongly affect the kinetic profiles. Thus, as shown for instance by Serpone *et al.*,[19] when the average number of electron–hole pairs per particle is inferior to ~0.5 the decays may follow first-order kinetics:

$$[c](t) = [c]_{t=0} e^{-k_r t} \tag{11}$$

On the contrary, when the average number of pairs per particle is greater than ~30, the decays may lead to kinetics that can be fitted by the second-order with a baseline eqn (10). To understand this behavior, it is necessary to recall that the derivation of classical kinetic laws implies a homogeneous distribution of reactants, which are present in a large enough number to consider their concentrations as continuous variables. In TA experiments, however, the number of electron–hole pairs per particle is usually much smaller than that limit, and thus the basic assumptions of classical kinetic models may not be valid. The correct treatment then involves stochastic kinetics tools, as was realized by Grätzel and coworkers in 1985.[80] By assuming a Poisson distribution of electron–hole pairs in colloidal TiO_2 particles, and an exponentially decaying survival probability for single electron–hole pairs, these authors obtained an equation governing charge carrier decays, which reduces to first-order and second-order rate laws at very low or very high initial charge carrier numbers, respectively.

Stochastic analyses also explain the origin of the *baseline* behavior. By modelling charge carrier recombination at the surface of TiO_2 colloidal particles through a computational approach, Grela and Colussi found

that the baseline shown by the decays is the inevitable consequence of recombination taking place in a 2-dimensional space, *i.e.* the particles' surface.[81] Electron–hole pairs which are initially at proximity will promptly recombine, while those far apart will remain for much longer times, giving rise to a phenomenon known as *fractal kinetics*, typical of low-dimensional media.[82] The consequence is that recombination at the surface *never* follows second-order kinetics: single electron–hole pairs decay exponentially, while multiple pairs decay through a second-order scheme where the rate *coefficient* (*i.e.* not *constant*) is time-dependent and asymptotically approaches a $t^{-1/2}$ dependence.

Generally, processes in which the rate coefficient k_r are time-dependent are said to follow *dispersive kinetics*, since, equivalently, it can be considered that there is not a unique value for (time-independent) k_r but rather a *distribution* of them.[83] A widespread example of a model based on this premise is that of Kohlrausch–Williams–Watts (KWW model).[84,85] Although it was initially employed in 1854 by Kohlrausch to describe the discharge of a capacitor,[84] it can also be successfully applied to chemical reactions with dispersive kinetics, by assuming a Lévy distribution (approximately, an asymmetric Gaussian-like distribution with a 'heavy' tail) for k_r.[86] The KWW function is then based on a superposition of first order reactions, each with a unique rate constant. Within this model the concentration of charge carrier follows a so-called *stretched exponential* behavior:

$$[c](t) = [c]_{t=0}\ \exp[-(k_r t)^{\beta}] \tag{12}$$

where β represents the distribution width ($0 < \beta < 1$). In the $\beta = 1$ limit the expression is reduced to the classical first-order one.

Similarly based on a first-order process, Albery and co-workers developed a kinetic model to fit the decay induced by interfacial electron transfer on semiconductor nanoparticles, in which the values of k_r follow a log-normal distribution:[87]

$$[c](t) \propto \int_0^{\infty} \frac{e^{-\frac{(\ln(k_r)-\ln(k_0))^2}{\gamma^2}}}{k_r} e^{-k_r t} \mathrm{d}k_r \tag{13}$$

where γ characterizes the distribution width and k_0 is the mean rate coefficient. As γ approaches zero, the dispersion diminishes, and the model resembles a first-order exponential decay.

More recently, Sieland *et al.* have derived a fractal kinetic equation[88] which can be understood as a second-order scheme modified to account for dispersion in the rate constant values:[89]

$$[c](t) = \frac{[c]_{t=0}(1-h)}{[c]_{t=0} k_r t^{1-h} + (1-h)} \tag{14}$$

where h ($0 \leq h \leq 1$) is the parameter dictating the width of the distribution. By setting $h = 0$ the equation reduces to the classical second-order behavior (eqn (9)). This function has proven to correctly describe TA decays of TiO_2 powders in the 50 ns to 1 ms range. The motivation behind

this proposition is that fitting with the second-order with a baseline function is usually adequate only for short times windows, and the kinetic parameters obtained at different times depend strongly on the analyzed time window. This problem can be sorted out by fitting experimental decays covering wide time windows using the fractal function.

It can be readily seen that, at very long times, the right-hand side of the divisor in the fractal model (eqn (14)) can be neglected, reducing the expression to a power law dependence:[83]

$$[c](t) \propto t^{-\alpha} \tag{15}$$

where α could be associated with $1-h$ in the previous equation. Such function has, for instance, been used by Cowan *et al.*[7] to explain the behavior of electron and hole decays in the microsecond to second time range in nanocrystalline TiO_2 films under applied bias. From the physical point of view, the function has been rationalized on the basis of the so-called trapping – detrapping model of charge carrier transport, which, as continuous-time random walk simulations show,[90] yields the same kinetic profile. Briefly, the model is based in an energetic dispersion of trap states, which electrons sample by continuously being trapped at different states and later detrapped with the help of thermal energy. The assumption of an exponential density of trap states leads to a power law behavior for the recombination kinetics.[90,91]

In the following, we give a more detailed view on each of these models, together with selected applications.

4.2 Classical kinetics

Let us start with a simple case, a first-order reaction representing the decay of a charge carrier c (either an electron or a hole), with a rate constant k_r:

$$c \xrightarrow{k_r} (\text{recombination}) \tag{16}$$

The rate law for a first-order reaction in a homogeneous medium is given by:

$$-\frac{\mathrm{d}[c](t)}{\mathrm{d}t} = k_r[c](t) \tag{17}$$

The derivative here implies that $[c](t)$ is a continuous variable, *i.e.* that it can take infinitely many, uncountable values. This assumption is valid when dealing with a number of molecules comparable to the Avogadro's number, but as we will see below it is generally not adequate to describe the behavior of charge carriers in TA experiments, since, at most, only a couple hundred of them is formed per particle after the laser pulse. Putting that remark aside for the moment, the equation can be reordered and integrated to yield the familiar first-order equation of classical kinetics, also called *exponential decay*:

$$[c](t) = [c]_{t=0}e^{-k_r t} \tag{18}$$

This functional form could have physical grounds on the description of *geminate* charge carrier recombination. If thermal energy is too low for excitonic dissociation to occur, as could be caused by very low temperatures or by a low dielectric constant of the semiconductor, the photogenerated electron–hole pairs never dissociate into separate entities but instead remain bound as an exciton, which can nevertheless relax by radiative or non-radiative recombination. The exponential behavior is also commonly observed in TA decays when the average number of pairs per particles is very low.[19,35,80] An early example is that of Rothenberger and coworkers,[80] who studied TiO_2 colloids (12.0 nm diameter) in aqueous suspensions and found monoexponential decays at long times (*i.e.* low average number of electron–hole pairs per particle), as shown in Fig. 13.

It is interesting here to evaluate the effect of parallel decay channels. For instance, we can consider an additional parallel decay reaction with a different rate constant $k_{r,2}$, representing *e.g.* radiative and non-radiative recombination pathways:

$$c \xrightarrow{k_r} (\text{recombination}) \quad \text{and} \quad c \xrightarrow{k_{r,2}} (\text{recombination}) \tag{19}$$

The corresponding differential equation is now:

$$-\frac{\mathrm{d}[c](t)}{\mathrm{d}t} = k_r[c](t) + k_{r,2}[c](t) = (k_r + k_{r,2})[c](t) = k'_r[c](t) \tag{20}$$

which can then be integrated to obtain again an exponential decay, this time with a rate constant $k'_r = k_r + k_{r,2}$. It is clear then that a parallel decay channel does not change the kinetic profile but only its apparent rate constant.

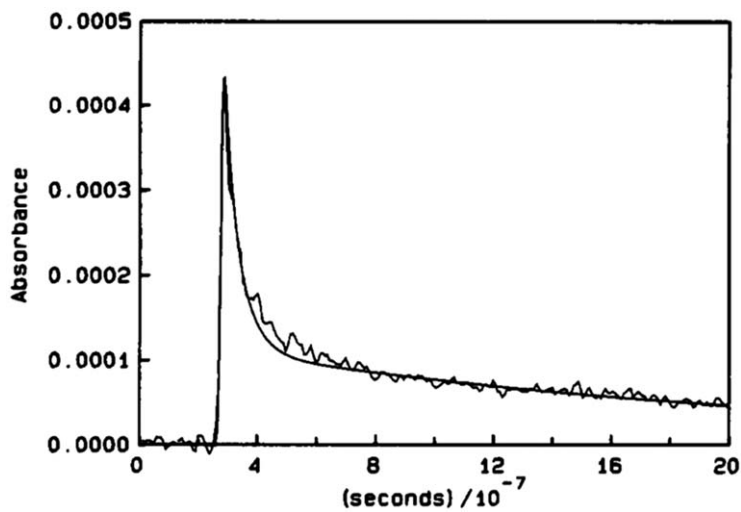

Fig. 13 TA decay observed at 800 nm for a colloidal TiO_2 suspension. At long times the profile follows a monoexponential decay. The calculated initial average number of photogenerated electron–hole pairs per particle is 0.85. Reproduced from ref. 80 with permission from American Chemical Society, Copyright 1985.

A different situation arises in the case known as *consecutive reactions*, for which a simple example could be the trapping of the carriers as a requisite for their recombination:

$$c_{\text{free}} \xrightarrow{k_r} c_{\text{trapped}} \xrightarrow{k_{r,2}} (\text{recombination}) \tag{21}$$

In this case we have:

$$\frac{\mathrm{d}[c_{\text{free}}](t)}{\mathrm{d}t} = -k_r[c_{\text{free}}](t) \tag{22}$$

$$\frac{\mathrm{d}\left[c_{\text{trapped}}\right](t)}{\mathrm{d}t} = k_r[c_{\text{free}}](t) - k_{r,2}\left[c_{\text{trapped}}\right](t) \tag{23}$$

Above we have shown the solution to equation (22):

$$[c_{\text{free}}](t) = [c_{\text{free}}]_{t=0}\, e^{-k_r t} \tag{24}$$

This result is then introduced in the eqn (23), and after some algebra[92] we get eqn (25),

$$\left[c_{\text{trapped}}\right](t) = \frac{k_r[c_{\text{free}}]_{t=0}}{k_{r,2} - k_r}\left(e^{-k_r t} - e^{-k_{r,2} t}\right) \tag{25}$$

considering $[c_{\text{trapped}}]_{t=0} = 0$ and $k_r \neq k_{r,2}$.

Now, if we assume that both c_{free} and c_{trapped} give rise to absorption, the observed TA signal $\Delta A(t)$ will be a linear combination of both concentrations (to account for possibly different absorption coefficients):

$$\Delta A(t) = A[c_{\text{free}}](t) + B\left[c_{\text{trapped}}\right](t) \tag{26}$$

After rearranging and grouping constants together, we get a functional dependence known as double-exponential or biphasic decay:

$$\Delta A(t) = Ce^{-k_r t} + De^{-k_{r,2} t} \tag{27}$$

Therefore, a mechanism of consecutive reactions is the simplest explanation for the observation of a double-exponential decay. Such type of behavior has been observed, for instance, by Horikoshi *et al.* for TiO_2 powders,[93] and by Zhang *et al.* for colloidal CdS suspensions (Fig. 14).[94]

So far, we have restricted ourselves to the first-order case and some derivations of it. In the non-geminate recombination case, as discussed in Subsection 4.1, electron and holes become independent entities roaming within the particles, and upon encountering each other may recombine. This situation could be, in principle, described by a second-order equal-concentration mechanism, for which the differential equation reads:

$$\frac{\mathrm{d}[c](t)}{\mathrm{d}t} = -k_r[c](t)^2 \tag{28}$$

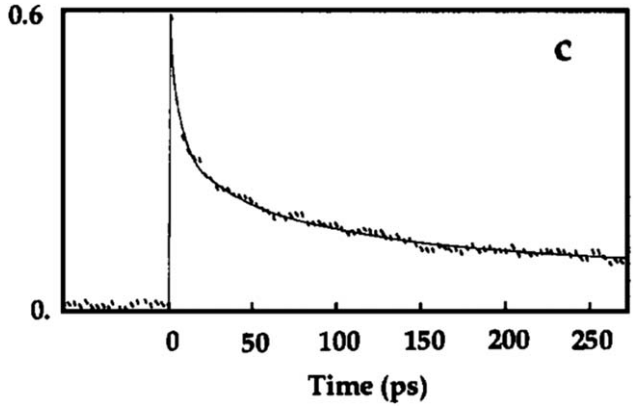

Fig. 14 TA decay observed at 780 nm for a colloidal CdS suspension. The continuous line shows a double exponential fit. Reproduced from ref. 94 with permission from Elsevier, Copyright 1994.

After rearrangement and integration, we get:

$$[c](t) = \frac{[c]_{t=0}}{[c]_{t=0} k_r t + 1} \tag{29}$$

There are many examples of its use from femtosecond to microsecond time windows.[19,32,79,95,96] Perhaps more interestingly, the derived second-order kinetic constants for recombination have frequently proved to be correlated with the photonic efficiency of photocatalytic processes over said materials.[31,97,98] Thus, even if the kinetic model follows a very basic premise, it still holds some predictive power which justifies its wide application.

4.3 Dispersive kinetics

In Subsection 4.2 we have assumed that the decay mechanisms follow either a first-order or a second-order elementary reaction step, occurring with a distinct rate constant. However, as mentioned above, the classical analysis assumes a spatially and energetically homogeneous reaction medium. This condition is not always met, and in fact many chemical systems deviate from the classical kinetics behavior. A typical example is the hydrogen abstraction reaction by alkyl radicals in organic glasses,[99] which would be expected to follow a simple (pseudo) first-order model, but instead has been empirically described by a function termed *stretched exponential* or Kohlrausch–Williams–Watts (KWW) function:[84,85]

$$[A](t) = [A]_{t=0}\, e^{-(k_r t)^{\beta}} \tag{30}$$

where $0 < \beta \leq 1$; $\beta = 1$ reduces the equation to the simple first-order case (eqn (18)). To understand the implications of this equation we can think of k_r not as a constant but instead as a function of time, $k_r = k'_r(t)$. Thus, the exponential factor in last equation can be rewritten as:

$$-(k_r t)^{\beta} = -k_r^{\beta} t^{\beta} = -k_r^{\beta} t^{\beta-1} t = -k'_r(t)\, t \tag{31}$$

This implies that the reaction follows a first-order equation, where the time-dependent rate *coefficient* $k'_r(t)$ equals $k_r{}^{\beta}t^{\beta-1}$, *i.e.*, the apparent rate constant gets progressively smaller as time passes.

An alternative view on the meaning of the stretched exponential function is obtained by assuming that the rate coefficient is time-independent, but instead of a unique value there is a distribution of them. We can understand this in the case of charge carrier recombination by recalling that the number of photogenerated species will most likely vary for different particles. Then, the stretched exponential function can be understood as the summation of simple exponential decays with different k_r values, representing an ensemble of particles where the different populations of electron–hole pairs lead to different individual recombination rates:[86,100]

$$[c](t) \propto e^{-(k_r t)^{\beta}} = \int_0^{\infty} g_{\mathrm{KWW}}(k_r, \beta) e^{-k_r t} \mathrm{d}k_r \tag{32}$$

Here $g_{\mathrm{KWV}}(k_r, \beta)$ is the probability distribution describing the possible values of k_r and their associated probability. The corresponding function for the KWW model is called a Lévy positive alpha-stable distribution. There are closed-form expressions only for a small set of β values, such as $\beta = 1/2$:[100]

$$g_{\mathrm{KWW}}\left(k_r, \frac{1}{2}\right) = \frac{1}{\sqrt{4\pi {k_r}^3}} e^{-\frac{1}{4k_r}} \tag{33}$$

More generally, it can be calculated as:[100]

$$g_{\mathrm{KWW}}(k_r, \beta) = \int_0^{\infty} e^{-u^{\beta}\cos(\pi\beta/2)} \cos\left[k_r u - u^{\beta} \sin\left(\frac{\pi\beta}{2}\right)\right] \mathrm{d}u \tag{34}$$

An equivalent expression exists in the form of a series expansion. From a qualitative point of view, the distribution function shows an asymmetric, approximately Gaussian shape, with a 'heavy' tail.

Some examples of the KWW model's application are those of Kamat *et al.*,[101] who studied electron injection from CdSe quantum dots to TiO_2 nanoparticles by monitoring their bleaching with femtosecond TA measurements; Durrant *et al.*,[37] who performed TA studies of electron transfer to oxygen from TiO_2 films using ethanol as hole scavenger; and Castellano *et al.*,[102] who observed delayed PL in pyrenyl-functionalized CdSe quantum dots, and, remarkably, found similar stretched-exponential behaviors both in time-resolved PL and TA spectroscopies.

A related model is that of Albery and coworkers,[87] which mainly differs from the KWW one by the assumption of a log-normal distribution of the first-order rate constant k_r. The attached physical meaning is that instead of a unique activation energy $\Delta G^{\dagger}$ there is a (Gaussian) distribution of them:[86]

$$\Delta G^{\dagger} = \Delta G_0^{\dagger} + \gamma x \mathrm{RT} \tag{35}$$

Here γ determines how strong the energy dispersion is (with $\gamma = 0$ leading to the simple first-order case), while the possible values of x follow a

Gaussian distribution function $p(x) \propto e^{-x^2}$. By substitution into the Arrhenius equation we get:[86]

$$k_r \propto e^{-\frac{\Delta G_0^{\dagger}}{RT} - \gamma x} = k_0 e^{-\gamma x} \tag{36}$$

where k_0 represents the mean rate constant. The rate law is obtained by summing over all possible values of k_r or, equivalently, all possible values of x:[86]

$$[c](t) \propto \int_{-\infty}^{\infty} e^{-x^2} e^{-k_0 t\, e^{-\gamma x}} \mathrm{d}x \tag{37}$$

By a change of variables this equation can be expressed in terms of the explicit form of the distribution function $g_{\mathrm{Albery}}(k_r)$, in a similar way as we did for the KWW model:[86]

$$[c](t) \propto \int_0^{\infty} g_{\mathrm{Albery}}(k_r) e^{-k_r t} \mathrm{d}k_r \tag{38}$$

with:

$$g_{\mathrm{Albery}}(k_r) = \frac{e^{-\frac{(\ln(k_r) - \ln(k_0))^2}{\gamma^2}}}{k_r} \tag{39}$$

The equation shows that k_r follows a log-normal distribution. In order to use the model for the fitting of experimental data, eqn (37) must be integrated. This was done by Albery *et al.* in the original paper using the extended Simpson's rule, giving as a result:[87]

$$\frac{[c](t)}{[c]_{t=0}} = \left(\frac{0.2}{3\pi^{\frac{1}{2}}}\right) \{2[f(0.1) + f(0.3) + f(0.5) + f(0.7) + f(0.9)] + f(0.2) + f(0.4) + f(0.6) + f(0.8) + e^{-k_0 t}\} \tag{40}$$

where:

$$f(\lambda) = \lambda^{-1} e^{-(\ln \lambda)^2} (e^{-k_0 t \lambda^{\gamma}} + e^{-k_0 t \lambda^{-\gamma}})$$

Then, both γ and k_0 can be used as fitting parameters.

Among other examples,[103] Draper and Fox have successfully applied the Albery model to fit TA decay kinetics of TiO_2 powders (Fig. 15).[104,105] These authors considered that the distribution in rate constant values more likely reflects the distribution of particle radii, instead of a distribution in the activation energies.

The model has also been recently employed by Peek *et al.*[106] to analyze the emission decay of Cr(VI) ions supported on silica (Fig. 16). Interestingly, they found a significant change in the dispersion width values γ, from 1.9 when the experiments were performed at room temperature to 3.8 when they were performed at 77 K, concluding that in the latter case there is a larger *distribution* of emitting sites, associated with a larger *number* of emitting sites under such conditions.

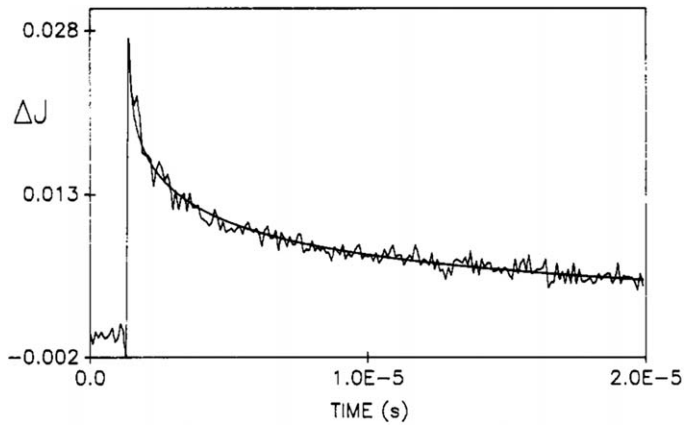

Fig. 15 TA decay observed at 480 nm for a TiO_2 suspension in reflectance mode. The line shows the fit to the Albery model. Reproduced from ref. 104 with permission from American Chemical Society, Copyright 1990.

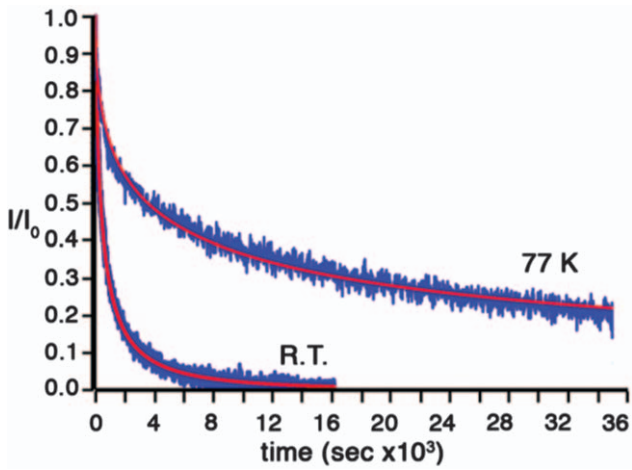

Fig. 16 Emission decays for Cr(VI) ions supported on SiO_2 observed at 626 nm, measured at two different temperatures. The red lines show fits to the Albery model. Reproduced from ref. 106 with permission from American Chemical Society, Copyright 2018.

The same concepts outlined above can be also applied to a second-order expression. Sieland and coworkers have proposed a *fractal model*, which can be interpreted in the same terms as the preceding ones. Starting from the classical second-order rate law (eqn (29)), and assuming a time-dependence on the rate coefficient k'_r:

$$k'_r(t) = k_r t^{-h} \tag{41}$$

We get the fractal model:

$$[c](t) = \frac{[c]_{t=0}(1-h)}{[c]_{t=0} k_r t^{1-h} + (1-h)} \tag{42}$$

By analogy with the previous model, h ($0 \leq h < 1$) can be understood as a parameter describing the dispersion in the recombination rates, related by the authors to spatial heterogeneity. The model was applied to TAS measurements on TiO_2 powders by monitoring the UV–Vis reflectance on the microsecond time range (Fig. 17). The main motivation for its derivation is that fitting the decays by a second-order treatment (*i.e.* by plotting the inverse of the differential reflectance *vs.* time) was only successful in selected time windows, and furthermore the resulting kinetic constants strongly depended on the chosen window. This has been observed by other authors,[107] and explained by Grela and Colussi in their stochastic treatment.[81] The advantage of the fractal model is that it can be robustly applied to different time windows and laser excitation energies, thus offering the possibility to perform quantitative comparisons. The inverse of k_r calculated by this approach has shown a strong correlation with the photonic efficiency for NO degradation over TiO_2,[108] although this correlation does not necessarily translate to other photocatalytic reactions (as shown for the acetaldehyde degradation).

For the derivation of the Albery model we assumed a dispersion in the activation energies, given by a Gaussian distribution for the values of x in eqn (35) and (36). If, instead of this distribution, they follow an exponential one $p(x) \propto e^{-x}$ (with $x \geq 0$) we have, in analogy with eqn (37):[86]

$$[c](t) \propto \int_0^\infty e^{-x} e^{-k_0 t\, e^{-\gamma x}} \mathrm{d}x \tag{43}$$

In the limit $k_0 t \gg 1$, the integral can be solved to get the *power law* time dependence:[109]

$$[c](t) \propto t^{-\alpha} \tag{44}$$

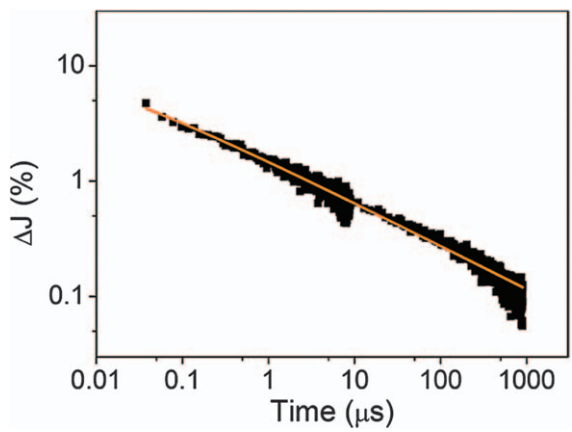

Fig. 17 TA decay observed at 500 nm for a TiO_2 powder in reflectance mode. The line shows the fit to the fractal model. Reproduced from ref. 88 with permission from American Chemical Society, Copyright 2017.

with $\alpha = 1/\gamma$ and $0 < \alpha \leq 1$. In the same way as for the KWW and Albery models, we can understand the power law decay as a summation of first-order processes with unique rate constants:[86]

$$[c](t) \propto t^{-\alpha} = \int_0^{\infty} g_{\text{Power Law}}(k_r) e^{-k_r t} \mathrm{d}k_r \tag{45}$$

$$g_{\text{Power Law}}(k_r) = \Gamma(\alpha)^{-1} \left(\frac{k_r}{k_0}\right)^{\alpha-1} \tag{46}$$

where Γ is the gamma function. Further physical insights into the power law dependence have emerged from stochastic models,[90,91] and will be covered in Subsection 4.4. It is noteworthy that, at long times, the fractal model (eqn (31)) reduces to a power law dependence for $[c](t)$.

An interesting application of this function has been done by Cowan *et al.*,[7] who performed TAS measurements on nanocrystalline TiO_2 electrodes under different applied potentials (Fig. 18). By manipulating the bias, they could selectively extend the lifetime of holes, allowing the water splitting reaction to compete with recombination. At potentials where no water splitting occurs the decay kinetics followed a power law function, whereas at more positive potentials the decays deviated from this behavior due to the consumption of holes by the oxygen evolution reaction. In the latter case the decays could be described as a combination of the power law function with a stretched exponential function (eqn (30)); the power law dominated at early times and was attributed to electron–hole recombination, while the stretched exponential function accounted

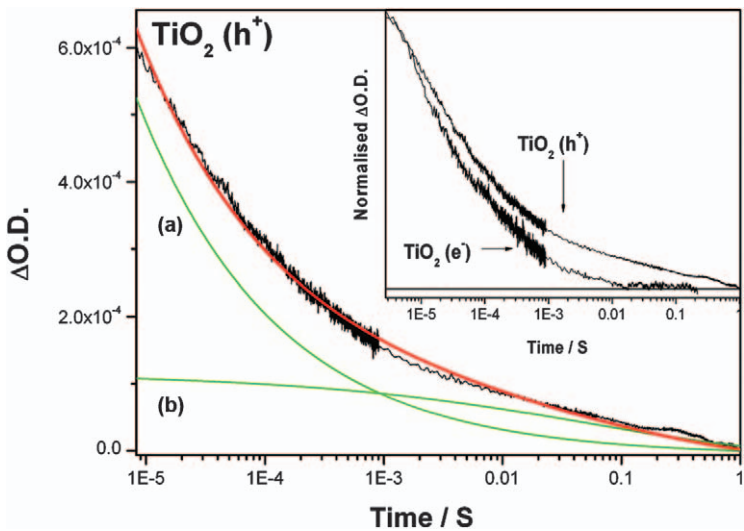

Fig. 18 TA decay observed at 460 nm for a nanocrystalline TiO_2 film. The red line shows the fit with a combination of a power law decay and a stretched exponential decay; the individual components are shown as green lines. The inset shows the normalized decay profiles assigned to photogenerated electrons and holes, illustrating the long lifetime of the latter due to the applied bias. Reproduced from ref. 7 with permission from American Chemical Society, Copyright 2010.

for longer time scales and was attributed to the reaction of holes with water.

4.4 Stochastic models

Both the classical and dispersive types of kinetic models consider the variable $[c](t)$ to be a continuous real-valued function of time. However, the number of photogenerated electron–hole pairs per particle after the laser pulse is an integer-valued variable, and the description of the process should take this into account. For instance, if 10 electron–hole pairs were generated in 100 particles, the classical view would assume that all particles would be populated with 0.1 pairs – a clearly unphysical situation. The correct picture of 90% empty particles and 10% particles with one electron–hole pair (neglecting here the small chance of particles populated with 2 or more pairs) calls for stochastic tools to be employed. An appropriate early treatment is that of Rothenberger *et al.*,[80] who derived a rate equation on the basis of some simple assumptions, the most important being that the survival probability of a single electron-hole pair in a semiconductor particle decreases exponentially with time, and that the initial distribution of pairs follows Poisson statistics. The main success of the expression is its ability to describe the kinetic profiles for the limiting cases of very low and very high initial occupancies, which result in first-order and second-order behaviors, respectively. These approximations were determined to be valid for an average pair number lower than 0.5 per particle and larger than 30 per particle, respectively.

A good example of the information that can be obtained from stochastic treatments is that of Grela and Colussi, who performed numerical simulations modelling electron–hole recombination (and reactive processes) on the surface of TiO_2 colloidal particles.[81] In this simple but elegant model, holes move randomly over the surface (modelled as a square 2D lattice) while electrons are immobile, since, for colloidal TiO_2, they are assumed to be located at deep traps. They conclude that the recombination process of multiple pairs does not follow simple second-order kinetics, but instead a dispersive second-order scheme where the rate coefficient asymptotically approaches a $t^{-1/2}$ dependence at long times. From the physical point of view, this behavior is the consequence of the disordered initial distribution of pairs on the particle's surface; those generated close together will promptly recombine, while those far apart will remain for much longer times. The simulations thus explain the baseline mentioned above (eqn (10)), due to electron–hole pairs that were generated far from each other and thereby display much longer lifetimes. In the case of one electron–hole pair per particle, the simulations show a first-order behavior, in line with experimental observations.[80] An important conclusion from this stochastic study is that the analysis of decay profiles by fitting with the second-order with a baseline function may lead to rate constants dependent on particle size or the initial number of electron–hole pairs, which may be difficult to rationalize. The stochastic analysis, remarkably, can fit TA decays for TiO_2 colloids of different sizes (Fig. 19), in the presence or absence of oxygen, and at small and large pulse intensities, using a *single* set of kinetic

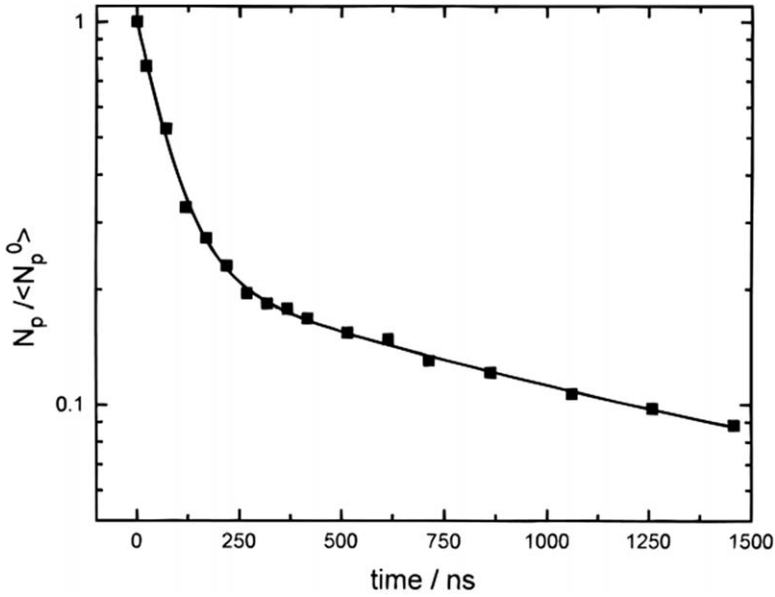

Fig. 19 Simulated TA decay employing a stochastic model of charge carrier recombination on the TiO_2 surface (continuous line), with an initial average number of electron–holes per particle of 0.85. Solid squares represent the experimental data of Rothenberger *et al.*[80] (shown in Fig. 13). Reproduced from ref. 81 with permission from American Chemical Society, Copyright 1996.

parameters. As a limitation, the assumptions in which the model is based (mobile holes, immobile electrons) are only valid for colloids obtained from the hydrolysis of TiO_2 precursors, and not, for instance, for pyrolytic microcrystallites such as Evonik P25 TiO_2, where electrons diffuse freely through the particles for long periods and resurface at different positions.[110] Therefore, in such case, multiple pair recombination is not expected to follow fractal kinetics, because the system is effectively three-dimensional.[81]

Additionally, random walk methods have often been used for the interpretation of recombination processes in dye sensitized solar cells,[90,91,111,112] and they also offer some interesting insights for the analysis of TA decays. The models mainly deal with charge transport in nanocrystalline semiconductor oxides, and the strong influence exerted by electron traps, which reduce conductivity by several orders of magnitude.[111] Furthermore, the discrete nature of the traps means that under certain conditions they can be ''filled'' or saturated, making the transport properties electron-concentration dependent.[113] A central aspect of these methods is thus the underlying transport model. One of the most commonly employed is the trapping – detrapping model,[112] where the electrons move *via* delocalized states in the conduction band, partially slowed by temporary trapping and subsequent release events aided by thermal energy. For both, rutile and anatase TiO_2 it has been stablished that electrons *self-trap* at Ti^{IV} lattice sites due to the distortion in the surroundings caused by the extra electron's charge, *i.e.*, due to small polaron formation.[114–116] The movement to another Ti^{IV} lattice site thus

involves overcoming this potential barrier. The most important consequence of the continuous time random walk simulations based on this model is that, given an exponential distribution of trap states, they reproduce the power law dependence on charge carrier recombination,[90] offering a strong physical background for its application. They are also useful to explain the strong dependence of recombination in dye – TiO_2 systems on applied bias, and may offer a remarkably good agreement with experimental data with only one adjustable parameter.[90]

Although stochastic models can be very useful for understanding the complex process behind recombination, a major difficulty comes from the fact that they seldom result in a compact analytic expression but rather require numerical analysis tools. Therefore, although the physical background may be somewhat obscured, it is usually much more straightforward to simply fit the experimental data with one of the equations derived from classical or dispersive kinetics.

5 Conclusions and final remarks

Transient absorption spectroscopy techniques, in which differential absorbance spectra are acquired with time resolutions from milliseconds down to femtoseconds, have proven extremely useful to study the dynamics of charge carriers in different semiconductor nanomaterials. Their time-resolved nature for very short scales make them a perfect match for photocatalytic processes, where the involved species are generally short-lived, and this is evidenced by the extensive mechanistic insights that have been obtained from their application.

The analysis of photocatalysts by TAS starts with the assignment of the transient spectrum features to photogenerated electrons and holes. The main strategy to differentiate their contributions is to employ scavenger compounds that selectively react with one of them. For instance, the observed transient spectrum in presence of a hole scavenger can be attributed to photogenerated electrons. It is important to bear in mind, however, that the presence of the scavenger will most likely have a strong influence in the chemical environment of the system. In general, there are no ''innocuous'' scavengers, and one should consider how the chosen scavenger may affect the system beyond their main function. As an alternative to chemical scavengers, if the semiconductor is configured as an electrode it is also possible to apply bias to selectively remove charge carriers: cathodic or anodic bias can be used to scavenge holes or electrons, respectively. In any case, it must be considered that the spectral features of the transient species are usually dependent on the experimental conditions.

The analysis of charge carrier kinetic profiles commonly entails the fitting of experimental data with an appropriate function. It is important to bear in mind that, in chemical kinetics, a good fit to a model cannot exclude the occurrence of other, perhaps more complex ones. In a best-case scenario, the strongest conclusion that could be reached is that the chosen model is *adequate* to describe the data. It is also important to recognize that, not rarely, kinetic schemes with different physical

justifications can result in similar or even indistinguishable functional shapes.[117] This problem may be exacerbated by the rather noisy profiles normally obtained in TA experiments.

From a more pragmatic point of view, one of the main reasons why TA spectroscopy is applied to photocatalytic materials is as a support to explain differential activities. Therefore, if the TA decay profiles of a series of materials can be described by a particular model, the as-obtained kinetic parameters could provide some insights into the charge carriers lifetimes, and consequently into their photocatalytic activities. Thus, even if the physical background justifying the election of the model may not be entirely clear, its application can nonetheless be useful. In such cases, however, the use of a more transparent parameter to characterize the decays should be considered, such as the time required to reach 50% of the initial TA signal.[65,118] The same is valid for decays which are not well described by any simple function, as could be the case, for instance, when charge carrier transfer to electron donors or acceptors substantially competes with their recombination.[119]

The typically low number of photogenerated electron–hole pairs per particle means that classical kinetics may not offer an adequate description, and stochastic models should be employed instead. Such models, even while (necessarily) simplifying the underlying processes, provide valuable tools for understanding TA kinetics. However, their implementation and application to experimental data is not as straightforward as simply fitting the data with an analytical function. Therefore, the latter method has been the preferred one for TA decays analyses.

The different models that are used for fitting would seem at first sight unconnected from each other. This is not really the case, and, as shown in Scheme 1, some associations can be made. The most basic vision comes from classical kinetics, from where we can obtain mono-exponential, bi-exponential, or second-order profiles depending on the reaction mechanism. Considering that the rate coefficient may be time-dependent, or, equivalently, that there is not a unique rate coefficient but rather a distribution of them, from the classical first order scheme we can

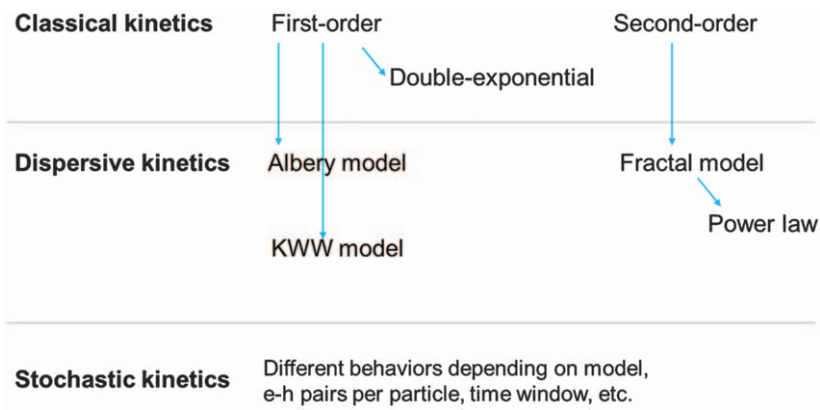

Scheme 1 Some relationships between kinetic models used for the analysis of TA decays.

obtain the KWW or the Albery models, depending on the rate coefficient distribution type. Similarly, assuming a dispersion of rate coefficients in the classical second order scheme, we obtain the fractal model. The power law profile, in turn, can be obtained from the fractal model at long time scales, and can also emerge from stochastic simulations based on the trapping – detrapping model.

Acknowledgements

Carsten Günnemann and Jenny Schneider acknowledge financial support from the Leibniz Universität Hannover within the program ''Wege in die Forschung II''. Additionally, Jenny Schneider thanks Alexander von Humboldt-Stiftung for financial support. Mariano Curti is grateful to the Deutscher Akademischer Austauschdienst (DAAD) together with the Ministerio de Educación, Cultura, Ciencia y Tecnología (Argentina) for his ALEARG scholarship. This work was supported by Saint-Petersburg State University *via* a research Grant ID 32706707.

References

1 J. Van Houten, *J. Chem. Educ.*, 2002, **79**, 548.
2 C. S. Ponseca, P. Chábera, J. Uhlig, P. Persson and V. Sundström, *Chem. Rev.*, 2017, **117**, 10940.
3 J. D. Simon, *Ultrafast Dynamics of Chemical Systems*, Springer Science & Business Media, New York, 2012.
4 J. Shah, *Ultrafast Spectroscopy of Semiconductors and Semiconductor Nanostructures*, Springer Science & Business Media, New York, 2013.
5 C. Luo, X. Ren, Z. Dai, Y. Zhang, X. Qi and C. Pan, *ACS Appl. Mater. Interface*, 2017, **9**, 23265.
6 J. Schneider, M. Matsuoka, M. Takeuchi, J. Zhang, Y. Horiuchi, M. Anpo and D. W. Bahnemann, *Chem. Rev.*, 2014, **114**, 9919.
7 A. J. Cowan, J. Tang, W. Leng, J. R. Durrant and D. R. Klug, *J. Phys. Chem. C*, 2010, **114**, 4208.
8 S. Selim, L. Francas, M. Garcia-Tecedor, S. Corby, C. Blackman, S. Gimenez, J. R. Durrant and A. Kafizas, *Chem. Sci.*, 2019, **10**, 2643.
9 A. Kafizas, R. Godin and J. R. Durrant, in *Semiconductors for Photocatalysis*, ed. Z. Mi, L. Wang and C. Jagadish, Elsevier Academic Inc, 2017, p. 3.
10 D. K. Pallotti, L. Passoni, P. Maddalena, F. Di Fonzo and S. Lettieri, *J. Phys. Chem. C*, 2017, **121**, 9011.
11 F. J. Knorr, C. C. Mercado and J. L. McHale, *J. Phys. Chem. C*, 2008, **112**, 12786.
12 R. E. Rex, Y. Yang, F. J. Knorr, J. Z. Zhang, Y. Li and J. L. McHale, *J. Phys. Chem. C*, 2016, **120**, 3530.
13 Y. Yamada and Y. Kanemitsu, *Appl. Phys. Lett.*, 2012, **101**, 133907.
14 I. A. Shkrob, M. C. Sauer and D. Gosztola, *J. Phys. Chem. B*, 2004, **108**, 12512.
15 D. Bahnemann, A. Henglein, J. Lilie and L. Spanhel, *J. Phys. Chem.*, 1984, **88**, 709.
16 Y. Tamaki, K. Hara, R. Katoh, M. Tachiya and A. Furube, *J. Phys. Chem. C*, 2009, **113**, 11741.
17 F. Le Formal, E. Pastor, S. D. Tilley, C. A. Mesa, S. R. Pendlebury, M. Grätzel and J. R. Durrant, *J. Am. Chem. Soc.*, 2015, **137**, 6629.
18 A. Hagfeldt and M. Grätzel, *Chem. Rev.*, 1995, **95**, 49.

19 N. Serpone, D. Lawless, R. Khairutdinov and E. Pelizzetti, *J. Phys. Chem.*, 1995, **99**, 16655.
20 T. Yoshihara, R. Katoh, A. Furube, Y. Tamaki, M. Murai, K. Hara, S. Murata, H. Arakawa and M. Tachiya, *J. Phys. Chem. B*, 2004, **108**, 3817.
21 V. Cristino, S. Marinello, A. Molinari, S. Caramori, S. Carli, R. Boaretto, R. Argazzi, L. Meda and C. A. Bignozzi, *J. Mater. Chem. A*, 2016, **4**, 2995.
22 B. Ohtani, *Catalysts*, 2013, **3**, 942.
23 R. W. Kessler and F. Wilkinson, *J. Chem. Soc., Faraday Trans. 1*, 1981, **77**, 309.
24 F. Wilkinson, *J. Chem. Soc., Faraday Trans. 2*, 1986, **82**, 2073.
25 C. J. Willsher, *J. Photochem.*, 1985, **28**, 229.
26 F. Wilkinson and C. J. Willsher, *Tetrahedron*, 1987, **43**, 1197.
27 P. Kubelka and F. Munk, *Z. Tech. Phys.*, 1931, **12**, 593.
28 T.-P. Lin and H. K. A. Kan, *J. Opt. Soc. Am.*, 1970, **60**, 1252.
29 A. Yamakata, J. J. M. Vequizo and H. Matsunaga, *J. Phys. Chem. C*, 2015, **119**, 24538.
30 A. Yamakata, H. Yeilin, M. Kawaguchi, T. Hisatomi, J. Kubota, Y. Sakata and K. Domen, *J. Photochem. Photobiol., A*, 2015, **313**, 168.
31 J. Schneider, K. Nikitin, M. Wark, D. W. Bahnemann and R. Marschall, *Phys. Chem. Chem. Phys.*, 2016, **18**, 10719.
32 J. Schneider and D. Bahnemann, *J. Phys. Chem. C*, 2018, **122**, 13979.
33 J. Schneider, K. Nikitin, R. Dillert and D. W. Bahnemann, *Faraday Discuss.*, 2017, **197**, 505.
34 J. Ravensbergen, F. F. Abdi, J. H. van Santen, R. N. Frese, B. Dam, R. van de Krol and J. T. M. Kennis, *J. Phys. Chem. C*, 2014, **118**, 27793.
35 Y. Tamaki, A. Furube, M. Murai, K. Hara, R. Katoh and M. Tachiya, *Phys. Chem. Chem. Phys.*, 2007, **9**, 1453.
36 A. Furube, T. Asahi, H. Masuhara, H. Yamashita and M. Anpo, *Chem. Phys. Lett.*, 2001, **336**, 424.
37 A. M. Peiro, C. Colombo, G. Doyle, J. Nelson, A. Mills and J. R. Durrant, *J. Phys. Chem. B*, 2006, **110**, 23255.
38 J. Tang, A. J. Cowan, J. R. Durrant and D. R. Klug, *J. Phys. Chem. C*, 2011, **115**, 3143.
39 Y. Tamaki, A. Furube, M. Murai, K. Hara, R. Katoh and M. Tachiya, *J. Am. Chem. Soc.*, 2006, **128**, 416.
40 A. Furube, in *Solar Energy Conversion: Dynamics of Interfacial Electron and Excitation Transfer*, The Royal Society of Chemistry, 2013, p. 281.
41 C. Colbeau-Justin and M. A. Valenzuela, *Rev. Mex. Fis.*, 2013, **59**, 191.
42 S. Biswas, J. Husek, S. Londo and L. R. Baker, *J. Phys. Chem. Lett.*, 2018, **9**, 5047.
43 F. Nunzi, F. Angelis, A. De and Selloni, *J. Phys. Chem. Lett.*, 2016, **7**, 3597.
44 D. Lawless, N. Serpone and D. Meisel, *J. Phys. Chem.*, 1991, **95**, 5166.
45 M. A. Henderson, *Surf. Sci. Rep.*, 2011, **66**, 185.
46 R. Memming, in *Electron Transfer I. Topics in Current Chemistry*, ed. J. Mattay, Springer-Verlag, Berlin Heidelberg, 1994, vol. 169, p. 105.
47 A. Yamakata, T. Ishibashi and H. Onishi, *J. Phys. Chem. B*, 2001, **105**, 7258.
48 C. O'Rourke, N. Wells and A. Mills, *Catal. Today*, 2018, DOI: 10.1016/j.cattod.2018.09.006.
49 D. Friedmann, H. Hansing and D. Bahnemann, *Z. Phys. Chem.*, 2007, **221**, 329.
50 X. Wang, A. Kafizas, X. Li, S. J. A. A. Moniz, P. J. T. T. Reardon, J. Tang, I. P. Parkin and J. R. Durrant, *J. Phys. Chem. C*, 2015, **119**, 10439.
51 H. Kisch, *Semiconductor Photocatalysis: Principles and Applications*, WILEY-VCH, Weinheim, 1st edn, 2015.
52 J. Schneider and D. W. Bahnemann, *J. Phys. Chem. Lett.*, 2013, **4**, 3479.

53 Y. Ma, S. R. Pendlebury, A. Reynal, F. Le Formal and J. R. Durrant, *Chem. Sci.*, 2014, **5**, 2964.
54 S. R. Pendlebury, M. Barroso, A. J. Cowan, K. Sivula, J. Tang, M. Grätzel, D. Klug and J. R. Durrant, *Chem. Commun.*, 2011, **47**, 716.
55 M. Zhu, Y. Mi, G. Zhu, D. Li, Y. Wang and Y. Weng, *J. Phys. Chem. C*, 2013, **117**, 18863.
56 D. W. Bahnemann, M. Hilgendorff and R. Memming, *J. Phys. Chem. B*, 1997, **101**, 4265.
57 Y. Murakami, J. Nishino, T. Mesaki and Y. Nosaka, *Spectrosc. Lett.*, 2011, **44**, 88.
58 P. V. Kamat, N. M. Dimitrijevic and R. W. Fessenden, *J. Phys. Chem.*, 1987, **91**, 396.
59 P. V. Kamat, T. W. Ebbesen, N. M. Dimitrijevic and A. Nozik, *Chem. Phys.*, 1989, **157**, 384.
60 T. Uchihara and M. A. Fox, *Inorg. Chim. Acta*, 1996, **242**, 253.
61 T. Uchihara, H. Oshiro and A. Kinjo, *J. Photochem. Photobiol. A Chem.*, 1998, **114**, 227.
62 N. Aiga, Q. Jia, K. Watanabe, A. Kudo, T. Sugimoto and Y. Matsumoto, *J. Phys. Chem. C*, 2013, **117**, 9881.
63 Y. Suzuki, D. H. K. Murthy, H. Matsuzaki, A. Furube, Q. Wang, T. Hisatomi, K. Domen and K. Seki, *J. Phys. Chem. C*, 2017, **121**, 19044.
64 Y. Yang, M. Forster, Y. Ling, G. Wang, T. Zhai, Y. Tong, A. J. Cowan and Y. Li, *Angew. Chem., Int. Ed.*, 2016, **55**, 3403.
65 S. R. Pendlebury, X. Wang, F. L. Formal, M. Cornuz, A. Kafizas, S. D. Tilley, M. Grätzel and J. R. Durrant, *J. Am. Chem. Soc.*, 2014, **136**, 9854.
66 S. R. Pendlebury, A. J. Cowan, M. Barroso, K. Sivula, J. Ye, M. Grätzel, D. R. Klug, J. Tang and J. R. Durrant, *Energy Environ. Sci.*, 2012, **5**, 6304.
67 F. M. Pesci, A. J. Cowan, B. D. Alexander, J. R. Durrant and D. R. Klug, *J. Phys. Chem. Lett.*, 2011, **2**, 1900.
68 W. Kim, T. Tachikawa, D. Monllor-Satoca, H. Kim, T. Majima and W. Choi, *Energy Environ. Sci.*, 2013, **6**, 3732.
69 Y. Yamada, T. Nakamura, S. Yasui, H. Funakubo and Y. Kanemitsu, *Phys. Rev. B*, 2014, **89**, 035133.
70 A. Yamakata, J. M. M. Vequizo and M. Kawaguchi, *J. Phys. Chem. C*, 2015, **119**, 1880.
71 D. Millers, L. Grigorjeva, V. Pankratov, V. A. Trepakov and S. E. Kapphan, *Nuc. Instrum. Methods Phys. Res. B*, 2002, **194**, 469.
72 P. V. Kamat and B. Patrick, *J. Phys. Chem.*, 1992, **96**, 6829.
73 E. A. McArthur, A. J. Morris-Cohen, K. E. Knowles and E. A. Weiss, *J. Phys. Chem. B*, 2010, **114**, 14514.
74 V. I. Klimov, C. J. Schwarz, D. W. McBranch, C. A. Leatherdale and M. G. Bawendi, *Phys. Rev. B*, 1999, **60**, 2177.
75 M. A. Khan, P. Maity, M. Al-Oufi, I. K. Al-Howaish and H. Idriss, *J. Phys. Chem. C*, 2018, **122**, 16779.
76 K. L. Corp and C. W. Schlenker, *J. Am. Chem. Soc.*, 2017, **139**, 7904.
77 R. Godin, Y. Wang, M. A. Zwijnenburg, J. Tang and J. R. Durrant, *J. Am. Chem. Soc.*, 2017, **139**, 5216.
78 S. K. Loeb, P. J. J. Alvarez, J. A. Brame, E. L. Cates, W. Choi, J. Crittenden, D. D. Dionysiou, Q. Li, G. Li-Puma and X. Quan, *et al.*, *Environ. Sci. Technol.*, 2019, **53**, 2937.
79 A. Furube, T. Shiozawa, A. Ishikawa, A. Wada, K. Domen and C. Hirose, *J. Phys. Chem. B*, 2002, **106**, 3065.
80 G. Rothenberger, J. Moser, M. Gratzel, N. Serpone and D. K. Sharma, *J. Am. Chem. Soc.*, 1985, **107**, 8054.

81 M. A. Grela and A. J. Colussi, *J. Phys. Chem.*, 1996, **100**, 18214.
82 R. Kopelman, *Science*, 1988, **241**, 1620.
83 A. Plonka, Y. A. Berlin and N. I. Chekunaev, *Chem. Phys. Lett.*, 1989, **158**, 380.
84 R. Kohlrausch, *Ann. Phys.*, 1854, **167**, 179.
85 G. Williams and D. C. Watts, *Trans. Faraday Soc.*, 1970, **66**, 80.
86 I. J. McNeil, D. L. Ashford, H. Luo and C. J. Fecko, *J. Phys. Chem. C*, 2012, **116**, 15888.
87 W. J. Albery, P. N. Bartlett, C. P. Wilde and J. R. Darwent, *J. Am. Chem. Soc.*, 1985, **107**, 1854.
88 F. Sieland, J. Schneider and D. W. Bahnemann, *J. Phys. Chem. C*, 2017, **121**, 24282.
89 A. Plonka, *Annu. Rep. Sect. C*, 1988, **85**, 47.
90 J. Nelson, S. A. Haque, D. R. Klug and J. R. Durrant, *Phys. Rev. B*, 2001, **63**, 205321.
91 A. V. Barzykin and M. Tachiya, *J. Phys. Chem. B*, 2002, **106**, 4356.
92 I. N. Levine, *Physical Chemistry*, McGraw-Hill, 6th edn, 2008.
93 S. Horikoshi, H. Tsutsumi, H. Matsuzaki, A. Furube, A. V. Emeline and N. Serpone, *J. Mater. Chem. C*, 2015, **3**, 5958.
94 J. Z. Zhang, R. H. O'Neil and T. W. Roberti, *Chem. Phys. Lett.*, 1994, **218**, 479–484.
95 D. P. Colombo and R. M. Bowman, *J. Phys. Chem.*, 1995, **99**, 11752.
96 R. Katoh, M. Murai and A. Furube, *Chem. Phys. Lett.*, 2008, **461**, 238.
97 A. Furube, T. Asahi, H. Masuhara, H. Yamashita and M. Anpo, *J. Phys. Chem. B*, 1999, **103**, 3120.
98 Y. AlSalka, A. Hakki, J. Schneider and D. W. Bahnemann, *Appl. Catal. B Environ.*, 2018, **238**, 422.
99 W. Siebrand and T. A. Wildman, *Acc. Chem. Res.*, 1986, **19**, 238.
100 D. C. Elton, ArXiv, 2018, **1**, arXiv:1808.00881v1.
101 I. Robel, M. Kuno and P. V. Kamat, *J. Am. Chem. Soc.*, 2007, **129**, 4136.
102 C. Mongin, P. Moroz, M. Zamkov and F. N. Castellano, *Nat. Chem.*, 2018, **10**, 225.
103 J. A. Tan, J. T. Rose, J. P. Cassidy, S. K. Rohatgi and K. L. Wustholz, *J. Phys. Chem. C*, 2016, **120**, 20710.
104 R. B. Draper and M. A. Fox, *J. Phys. Chem.*, 1990, **94**, 4628.
105 R. B. Draper and M. A. Fox, *Langmuir*, 1990, **6**, 1396.
106 N. M. Peek, D. B. Jeffcoat, C. Moisii, L. van de Burgt, S. Profeta, S. L. Scott and A. E. Stiegman, *J. Phys. Chem. C*, 2018, **122**, 4349.
107 A. Yamakata, T. A. Ishibashi and H. Onishi, *Chem. Phys. Lett.*, 2001, **333**, 271.
108 F. Sieland, J. Schneider and D. W. Bahnemann, *Phys. Chem. Chem. Phys.*, 2018, **20**, 8119.
109 M. Tachiya and A. Mozumder, *Chem. Phys. Lett.*, 1975, **34**, 77.
110 J. M. Warman, M. P. De Haas, P. Pichat and N. Serpone, *J. Phys. Chem.*, 1991, **95**, 8858.
111 J. A. Anta, *Energy Environ. Sci.*, 2009, **2**, 387.
112 J. Nelson and R. E. Chandler, *Coord. Chem. Rev.*, 2004, **248**, 1181.
113 K. Schwarzburg and F. Willig, *Appl. Phys. Lett.*, 1991, **58**, 2520.
114 I. G. Austin and N. F. Mott, *Adv. Phys.*, 2001, **50**, 757.
115 C. Di Valentin and A. Selloni, *J. Phys. Chem. Lett.*, 2011, **2**, 2223.
116 S. Yang, A. T. Brant, N. C. Giles and L. E. Halliburton, *Phys. Rev. B*, 2013, **87**, 125201.
117 Á. Balogh, G. Lente, J. Kalmár and I. Fábián, *Int. J. Chem. Kinet.*, 2015, **47**, 773.
118 J. Tang, J. R. Durrant and D. R. Klug, *J. Am. Chem. Soc.*, 2008, **130**, 13885.
119 A. Yamakata, T. A. Ishibashi and H. Onishi, *J. Mol. Catal. A: Chem.*, 2003, **199**, 85.